NUMERICAL INVESTIGATIONS ON THE AERODYNAMICS OF GROUND VEHICLES IN PLATOON USING THE FASTBACK DRIVAER MODEL

by

Sudhan Rajasekar

A thesis submitted to the faculty of
The University of North Carolina at Charlotte
in partial fulfillment of the requirements
for the degree of Master of Science in
Mechanical Engineering

Charlotte

2018

Approved by:

_____

Dr. Mesbah Uddin

_____

Dr. Christopher Vermillion

_____

Dr. Peter T. Tkacik

ABSTRACT

SUDHAN RAJASEKAR. Numerical investigations on the aerodynamics of ground vehicles in platoon using the fastback drivaer model. (Under the direction of DR. MESBAH UDDIN)

Work concerning aerodynamic optimization of isolated vehicle shapes is available in abundance in existing literature, unlike vehicle interaction studies. Due to its simplicity, all previous studies aimed at understanding the aerodynamic interference effects were carried out primarily using the Ahmed body as the vehicle model. Wind tunnel studies on vehicle interferences using an actual car geometry would be expensive and complicated owing to the geometric limitations of the test facility and the associated difficulties in measurement techniques employed. The work presented in this thesis explores the aerodynamic prediction capabilities of popular turbulence models, used in present-day computational fluid dynamics simulations, using a realistic car model in a platoon. A simulation methodology is first developed using a tandem arrangement of surface-mounted cubes considering the availability of experimental data for CFD correlation and validation. The influence of turbulence model closure coefficients on the prediction capabilities is tested first and a combination of modified coefficients is selected that improves the overall predictions of the SST $k - \omega$ turbulence model. Validation studies reveal the inability of the Unsteady Reynolds-Averaged Navier-Stokes(URANS) models to resolve the far wake and hence its frailty in simulating multiple body interactions. Improved Delayed Detached Eddy Simulations(IDDES) models, on the other hand, are able to resolve the wakes with a reasonable accuracy. The simulation methodology is then applied to the fastback DrivAer model at different longitudinal spacings. The results show that, as the longitudinal spacing is reduced, the trailing car's drag is increased while the leading car's drag is decreased. The current study supports the prior explanation of vortex impingement as the reason for drag changes. Unlike Ahmed bodies, the trailing model does not return to

an isolated state at two car-length separation. The resolution of the far wake of a detailed DrivAer model and its implication on the CFD characterization of vehicle interaction aerodynamics needs further investigations.

ACKNOWLEDGEMENTS

Thank you Mom!

TABLE OF CONTENTS

LIST OF FIGURES

LIST OF TABLES

CHAPTER 1: INTRODUCTION

Road vehicle aerodynamics poses one of the most complex problems that needs a greater understanding in spite of numerous studies in this area over the past few decades. With the increase in demand and a diminution in supply of fossil fuels, reduced energy consumption has become of prime importance in the automotive industry. Vehicle manufacturers have focused on reduction of drag which is directly attributed to the fuel economy and top speed of the vehicle. Vehicle platooning has been documented as one of the ways outside design changes to reduce overall drag of a fleet and thereby reducing the total fuel consumption since the 70s [2]. Drag is of prime concern in the motorsports industry as well.

A road vehicle in isolation can be fundamentally considered as a bluff body and research into optimizing this bluff body has provided us with information in abundance not only pertaining to reduction of total drag but also the influence of aerodynamics on the performance of the vehicle [3]. Detailed investigation of flow fields reveal that the entirety of the flow structures are not macroscopically stable but consist of dynamic components as well [4]. A deeper understanding of the implications of these dynamic components have intrigued an interest pertaining to the influence of turbulence on road vehicles. Turbulence can either be from free-stream turbulence levels or as exerted by some external sources, among which proximity of other vehicles on road being the most prominent. The complex flow field around the vehicle defines the degree to which these sources impact the vehicle and its complexity is further intensified by the presence of an additional vehicle. In recent years, road vehicle population has exceeded available road network resulting in a decline in traffic throughput; raising numerous related concerns. Vehicle interaction is more influential

when it comes to racing as it involves high speed overtaking and with higher speed, the effect is quadrupled. This has led to increased concerns in the racing industry, especially related to safety, considering the scarcity in available resources with regard to this phenomena.

A study of this turbulence interaction proves vital as this problem is very complex and it is seen that it becomes expensive and more difficult to be conducted in a wind tunnel [5]. Computational Fluid Dynamics (CFD) is of growing interest in recent years with the advancement in computational resources and the ability of CFD to solve complex flow situations with considerable accuracy. In spite of the proven credibility of scale resolving simulations, Reynolds Averaged Navier-Stokes (RANS) simulations are preferred from an industrial stand-point on account of its faster turn-around time and cost effectiveness. However, RANS models fail to reproduce certain "flow features" and it has already been proven that mesh refinement is not the solution in regards to such models.

Although vehicle platoons and drafting has been studied since the late 70s, not a lot of data has been published, both experimental and computational, with regard to vehicle interaction over the past years. Most of the studies have been quasi-steady cases, wherein the approaching vehicle is moved in steps and a time-averaged flow field is analyzed, with a few transient studies published[4, 6, 7]. The transient studies are done using a sliding mesh technique which is computationally demanding as a very fine mesh is required throughout the domain.

1.1   Motivation

When two bodies are in close proximity to each other, the flow field around them interact with each other creating gust loads and excitations about their axes. Researchers have attempted in understanding the underlying phenomena during such interactions and have been able to provide important data on flow features and force coefficients for several forms of bluff bodies. These studies are often carried out as

quasi-steady approaches, where the bodies are kept at constant relative to each other and a steady flow field analyzed. These studies have provided us with great insight into deconstructing mean flow phenomena. Quasi-steady approaches are based on two basic assumptions:

1. Flow conditions remain steady throughout

2. The effects of relative velocity is negligible

The influence of longitudinal spacing, relative velocity and transient flow conditions such as a crosswind on vehicle interaction have been documented in several studies. Yamamoto and Nakagawa conducted a dynamic study on 1/10th scale models and observed that even a small relative velocity could significantly affect the flow field and the resultant forces acting on the vehicles. They also concluded that for k<0.25, where k is the ratio of relative velocity to the velocity of the lead vehicle, the problem could be modeled statically and that the dynamic effects could be neglected. Gillieron and Noger[8] ran experiments and CFD using an overtaking test bench for various relative velocities with 1/5th scale Ahmed models. Their results indicated that side forces can be 120% higher than predicted by quasi-steady techniques when k=0.32.

From the results of Noger's experiments it is found that during passing, the rear vehicle is affected by unsteady aerodynamic effects after certain threshold velocity ratio. The transient case they presented produced lower aerodynamic coefficients than that of the quasi-steady case. Force and static pressure data on the vehicles have been presented to validate the phenomena. They suggest that aerodynamic forces on the overtaking vehicle becomes velocity dependent when k>0.2. The data presented for k≈0.5 exhibited significantly different behavior from that of the quasi-steady analysis. Noger also presented data that supports the influence of crosswinds during transient situations and the importance of transient studies.

Corin et al.'s 2D study of the overtaking maneuver demonstrated the quasi-steady

approach's failure to capture the dynamic flow interactions and variations in aerodynamic forces. They stated that quasi-steady methods could only capture the pseudo-periodic variations which indicate that quasi-steady analysis is unsuitable for modeling such complex on-road scenarios[9].

Watts in his CFD study[7] also predicted similar trends in force coefficients with Ahmed bodies and more complicated trucks. Watts' predictions were similar to Paglierella[4] associating the reason for the trends to the lead vehicle wake structures, thus the vortex interactions. Watts used both URANS and DES to model the turbulence and his results explained the discrepancies in Rajamani's CFD results[31]. Rajamani's CFD results had issues where at a spacing of 2L, the Ahmed bodies did not revert to the isolated state values.

The author in this study decided to use overset meshing technique because of the possibility to transform the mesh into a transient case without any hassle and the cost-effectiveness of the overset grids. The advantages of overset mesh method in such scenarios has already been validated in Chellaram's[10] thesis work on an overtaking maneuver using Ahmed bodies. Furthermore, the data available on drafting or multiple vehicle interactions are only based on simplified models like the Ahmed body[15]. Heft et al.,[11] highlighted the difference in flow features between such simplified models and an actual vehicle in their work. Specifically, the classical representation of flow structures were modified as generic models like Ahmed bodies fail to reproduce the A-pillar vortices and their downstream development. The complex underbody of a ground vehicle is also drastically different from that of the smooth underbody of Ahmed body which would have a significant effect on the wake length.

The work presented in this thesis investigates the possible influence of this difference in flow structure on the outcomes during a drafting situation and also try to improve the predictions of the turbulence modeling techniques that are currently available. The main focus of this thesis work is to provide the CFD community with

a computationally less expensive method of simulating flows around bluff bodies and vehicle geometries with considerable accuracy and also to provide insights into simulating such complex flows involving multiple bodies. The author also aims to develop a meshing strategy that is computationally effective and is fluid enough to be easily transferred from a quasi-steady setup to a transient setup.

1.2   Thesis Outline

The theis is organized in the following manner: Chapter 2 discusses the background of vehicle interactions and outline relevant work that has been compiled. Chapter 3 details turbulence modeling and its significance in CFD studies. Chapter 4 provides information on the finite difference code used to solve the simulations and the meshing strategy developed and other important details regarding the simulation setup. Chapter 5 contains the results and conclusions from the investigations on the prediction capabilities of turbulence models in a simulation involving multiple bodies. A simple bluff body, the surface-mounted cube, has been used in this study to analyze near and far wake resolutions of different turbulence models. Chapter 6 applies the process developed in Chapter 5 to investigate the possibility of resolving far wake of a realistic road vehicle, the DrivAer model, both in isolation and in platoon. Chapter 7 concludes the thesis with a summary and outlines scope for future analysis of the work.

CHAPTER 2: BACKGROUND

Road vehicle aerodynamics design and its vitality surfaced and was brought to the fore by the crude oil crisis(1973) until which design to reduce drag was secondary and was stagnant. It was made clear from research that aerodynamic design played a crucial role not only in reducing the energy consumption but also expanded to other vehicle parameters such as handling, noise, cooling and the like [12]. Research on ground vehicle aerodynamics, fundamentally assuming them as bluff bodies moving in close proximity to ground surface, began in early 70s with a multitude of reference bluff bodies used. The main focus in the earlier periods of research was to bring down drag, the primary dictator of performance and fuel economy. More recently, studies concerning the effects of upstream turbulence have been gaining interest.

Experimental wind-tunnel tests were predominant in the early periods of vehicle research owing to the limitations on the availability of computational resources as well as the limitations on the numerical models itself. Most numerical models were developed based on the tests on canonical flows and hence could not perform as good when it comes to solving more complex flow problems, in this case vehicle wakes. Flow around a road vehicle involves resolving both boundary layer development on the surface of the vehicle and the high-vorticity wakes left behind. As we know, this is many folds complex to that of canonical flows and hence turbulence models suffer in such scenarios failing to produce well correlated predictions.

The study of tandem vehicles and other relevant phenomena originated in the motorsports industry as *slipstreaming* was often and more common during overtaking while racing. On average, about 49 overtakes per GP was recorded during the 2016 Formula One season mounting to a total of 1030 overtakes through the whole season.

A net drag reduction was reported by Horner in 1965 using tandem discs and was further analyzed by Koenig and Roshko[4]. An initiative to understand the phenomena was first done by Romberg et al., [13] citing net convoy drag gains in close proximity. Hucho insisted that the effect of drag reduction on fuel consumption is overstated with the focus of most studies only on steady-state driving. But, it is inferred from studies that there is considerable opportunity to benefit from such on-road situations and realize significant reductions in energy consumptions.

2.1   DrivAer Reference Geometry

Vehicles are classified into three basic forms based on their characteristic flow topology for transfer of useful research data. Vehicle forms have been evolving since the early 1900s from the streamlined torpedo and boat-tail forms until Kamm et al., disproved the necessity of a streamlined tail and introduced the "Kamm tail", with a blunt rear end, generating satisfactory aerodynamic performance. The resulting wake flow is complex enough that it is being studied to present date. The three classical forms of passenger cars are the following and are represented with their basic flow topologies in Figure 2.1.

1. Notchback

2. Fastback

3. Squareback
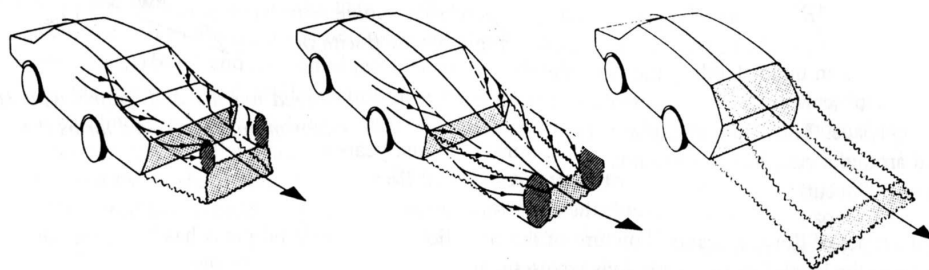
Figure 2.1: Flow topology of notchback(left), fastback(middle) and squareback(right) forms [12]

Vehicle aerodynamics is complex because of the compact dimensions and aspect ratios which lead to increased probability of substantial interaction between complex, three-dimensional flow phenomena. Hence, a holistic approach towards understanding the flow phenomena around a ground vehicle has to be considered instead of studying flow off of each component in isolation.

The fastback geometry can be represented by a 25° Ahmed body and has been extensively researched over the last few decades. The data at disposal regarding the geometry is is abundance and hence this research will focus on this specific configuration. The salient flow features thought typical of a fastback configuration back in 1976 is prensented in Figure 2.2. Increasingly complex flow phenomena have been associated with the reference geometry since then while Hucho has captured salient features of the flow.
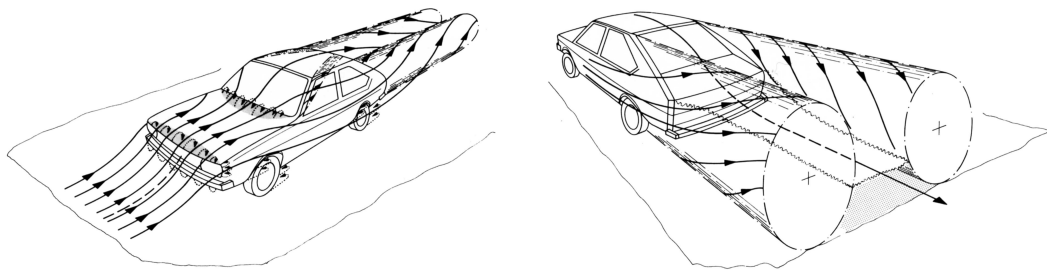
Figure 2.2: Characteristic flow over a fastback-type vehicle [3]

DrivAer model was added recently to the open source car geometries as a result of a joint project between Audi AG, BMW and the Institute of Aerodynamics and Fluid Mechanics of the Technische Universitat Munchen (TUM)[14, 1, 11]. The reference geometry consists of three configurations to cover all the classical forms described earlier as a modular type geometry as shown in Figure2.3. Experimental data was made available by the same research group and have provided global load data and surface pressure information in key areas of the vehicle for all forms. For each configuration, a multitude of variants were also made available, tested and the data was presented. The effect of ground simulation on the vehicles was also tested and documented.
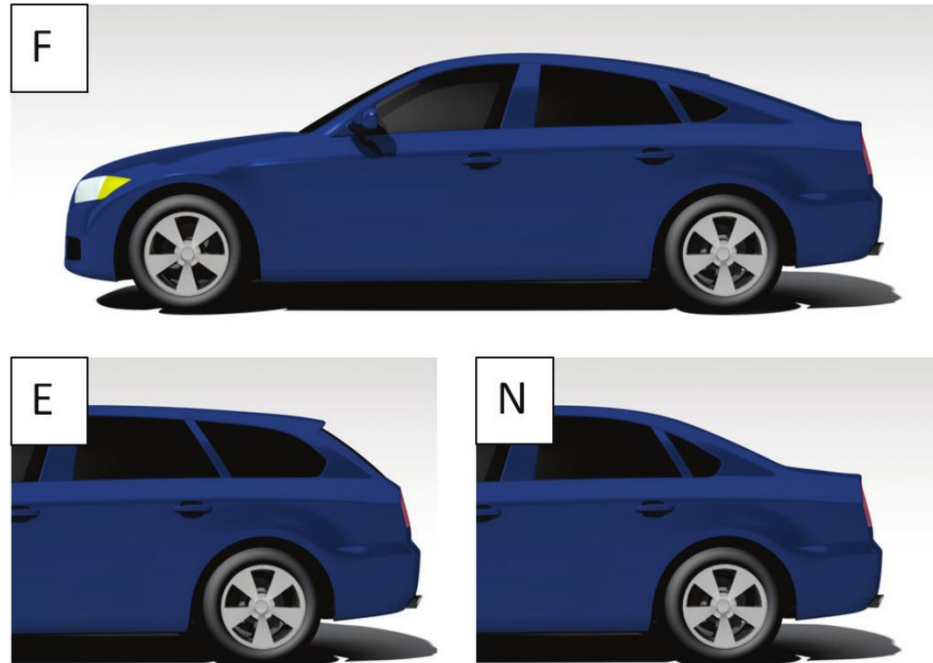
Figure 2.3: DrivAer Reference Geometry

TUM has also conducted numerical investigations on the fastback configuration with k-ω SST model and the results were compared with experimental data [11]. A certain amount of error was observed in their pressure distribution over the top of the vehicle although the force coefficient prediction showed excellent agreement with wind tunnel data.

DrivAer geometry is so similar to on-road vehicles and is very complex that the flow separates and reattaches four times along the span of the vehicle before finally separating at the trailing edge of the base into the wake. There are stagnation areas at the nose and at the base of the windshield (cowl). The flow around the geometry can be split into quasi-steady two-dimensional and unsteady three-dimensional. The stagnation regions mentioned earlier and the two recirculating vortices formed by the flow separated from the trailing edges of the base are quasi-steady in nature. Two votices developed from the base of the A-pillar and the C-pillar are highly unsteady and 3D in nature. The A-pillar vortex developing detaches before the roof, gains strength as it is transported over the roof; forming a cylindric vortex structure at the

junction betwen the roof and the rear window; and it does not affect the flow field further downstream. The C-pillar vortex though, detaches as the flow accelerates over the C-pillar and is extended into the near wake as it creates a downwash. These are rich in kinetic energy and is fed by the shear layers off the C-pillar. The core of these vortices are characterized by reduced static-pressure and it creates a region of low pressure on impingement, at the penalty of induced drag[15, 12].

2.2   Bluff Body - Cubes on ground

Considering the computational resources available and the time limit posed, studies on the CFD setup and turbulence modeling was conducted on cubes attached to the ground to understand the complex wake generated by bluff bodies. The knowledge gathered from these studies are then transfered onto the setup of the 40% scaled DrivAer geometries.

Flow around a cube and a DrivAer geometry is analogous in a sense that both geometries induce strong separation of flow past them, a highly complex wake flow about the base region and 3D high energy vortices extending into the far wake influencing the wake flow. This study is not proposing in any sense that these two flows can be considered one and the same. The focus here is on investigating the ability of turbulence models in resolving such complex high kinetic energy wakes with 3D vortices and cubes are chosen in the motive of saving computational cost and time.
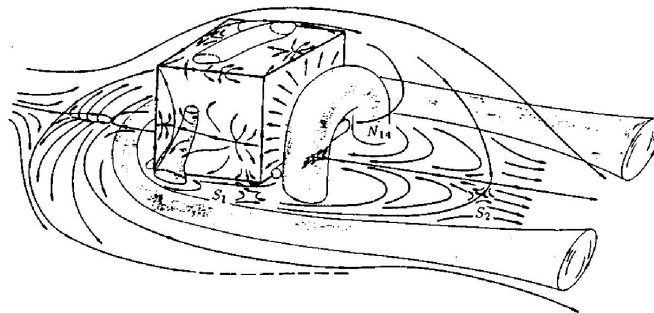
Figure 2.4: A schematic representation of the main macroscopic flow features[16]
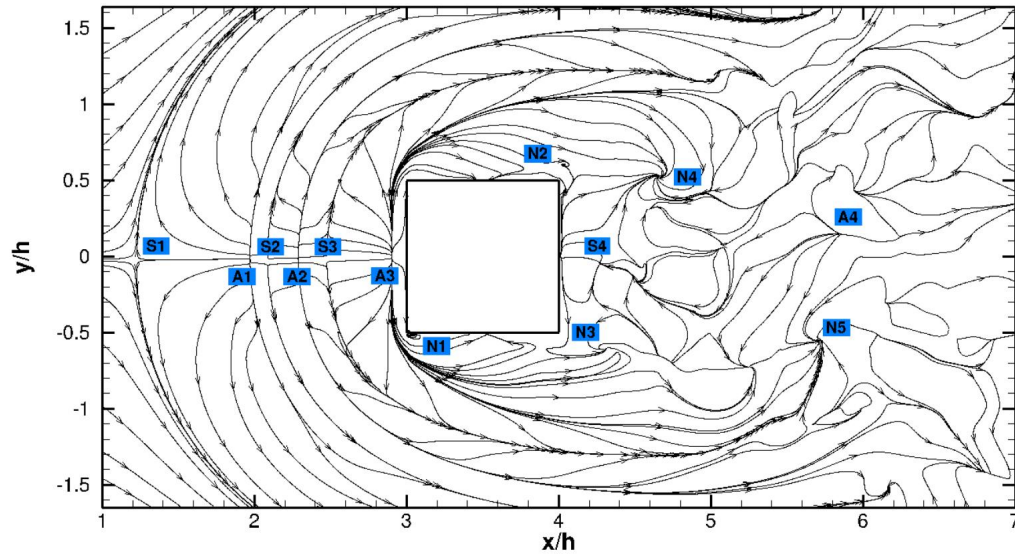
Figure 2.5: Instantaneous Streamlines near the wall at z/h=0.003[17]

Figure 2.4 shows the macroscopic flow features around a surface mounted cube as presented by Hussein and Martinuzzi[16] and figure 2.5 shows the instantaneous streamlines presented by Curley and Uddin[17] in their DNS work. A series of work were published after the the first experimental work by Martinuzzi and Tropea[18] over low and moderate Reynolds numbers. The flow patterns observed indicate that the flow separates at the front of the cube along the edges. A horse-shoe vortex system consisting of a series of up to six vortices was identified by Curley as observed by Hunt et al.[19] These are highly sensitive to upstream flow parameters[19, 20]. Recirculations along the sides of the cube and downstream of the cube, marked N2 and N4, were also presented by Curley, as in figure, which matched well with other experimental studies suggesting an arch-shaped vortex downsteam of the cube. The separations from the top and sides of the cube are the reason for the generation of this arch-shaped vortex and N4 marks the base of the vortex. Two counter rotating vortices are observed 0.3h downstream of the cube, where h is the cube height, entraining fluid behind the cube. The huge recirculation bubble behind the cube was found to reattach at about 1.7h. This reattachment point was documented to be

influenced by the boundary layer thickness upstream of the cube[17]. The velocity profiles around a surface mounted bluff body was presented by Castro, which was used in the earlier stages of the study to validate the CFD setup used.

Numerous studies have been published analyzing the flow around a surface mounted bluff body. Hence, this would be the perfect test case to understand the turbulence models and to generate a test method to be implemented in a more complex model. Some of the other notable works on surface-mounted bluff bodies include the works of Iaccarino et al., Rodi[21], Yakhot et al.[22], Bearman[23] and Martinuzzi's work with several other researchers[18, 24, 25]. Martinuzzi's work on tandem bluff bodies is used to validate this work.

2.3   Influence of Turbulence

Freestream turbulence intensity(I) can be defined as the level of "*gustiness*" in the flow [26]. The relevance of free stream turbulence on bluff body flows are well documented by Bearman[23] and Nakamura[27]. An increase in freestream turbulence can affect turbulent transitions in boundary layers and mixing between shear layers in the near wake and hence reducing the base pressure.

The flow field is made turbulent and drastic gust loads are induced while drafting[28]. In the study of aerodynamic interaction between commercial vehicles by Gotz[29], he found that when a convoy of vehicles are driven at speeds of 80 km/h with an inter-vehicle spacing of 40 m, drag force could go down by 20% for the second vehicle, 30% for the third. Abdel Azim and Abdel Gawad[30] experimented with 1/60 scaled models of Mercedes Benz C 280 to study the flow in the inter-vehicle spacing at Reynolds numbers 6000 and 11000. They found that three modes existed in the flow: wake impingement, steady vortex wake and low-pressure cavity. The separated shear layers from the lead model either impinged on the trail model or rolled up to form a steady vortex based on the car length at lower Re, while it reattached on the trail model surface forming a low-pressure cavity in the inter-vehicle spacing as Re is increased.

They noticed considerable drag savings for the trail model at close spacings reaching the lowest possible drag in the low-pressure cavity mode.

Vino and Watkins[6] conducted an experimental study on Ahmed bodies, with a real slant angle of 30°, in tandem to understand the effect of inter-vehicle spacing on flow around the models. They reported that vortex interaction between vehicles play a vital role in determining the force coefficients of the vehicles and that significant drag penalties are experienced by the models at close spacing (as seen is Figure2.6) especially less than one model(car) length. They also reported no significant change in the trailing model wake and hence, stipulated leading model wake to be the reason for these force coefficient changes. Rajamani's CFD studies[31] on Ahmed models and pickup truck models produced C_D trends similar to that of Vino and Watkins[6].
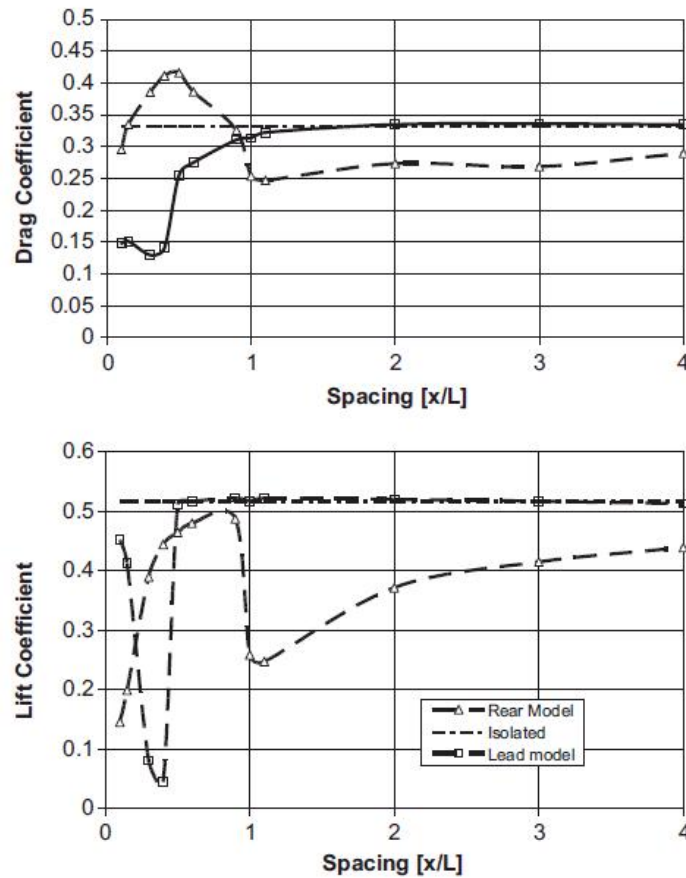
Figure 2.6: Drag and Lift coefficients as presented by Vino and Watkins for a platoon using Ahmed bodies[6]

In order to better understand the phenomena, Paglierella[4] experimented with multiple Ahmed bodies in a convoy arrangement. He studied a range of spacing varying between 2L to 0.125L. Paglierella interestingly concluded that in a convoy/drafting situation, where the bodies are perfectly in line with each other, the lead body experienced drag reduction throughout the spacing range while the trail body experienced an opposite trend.
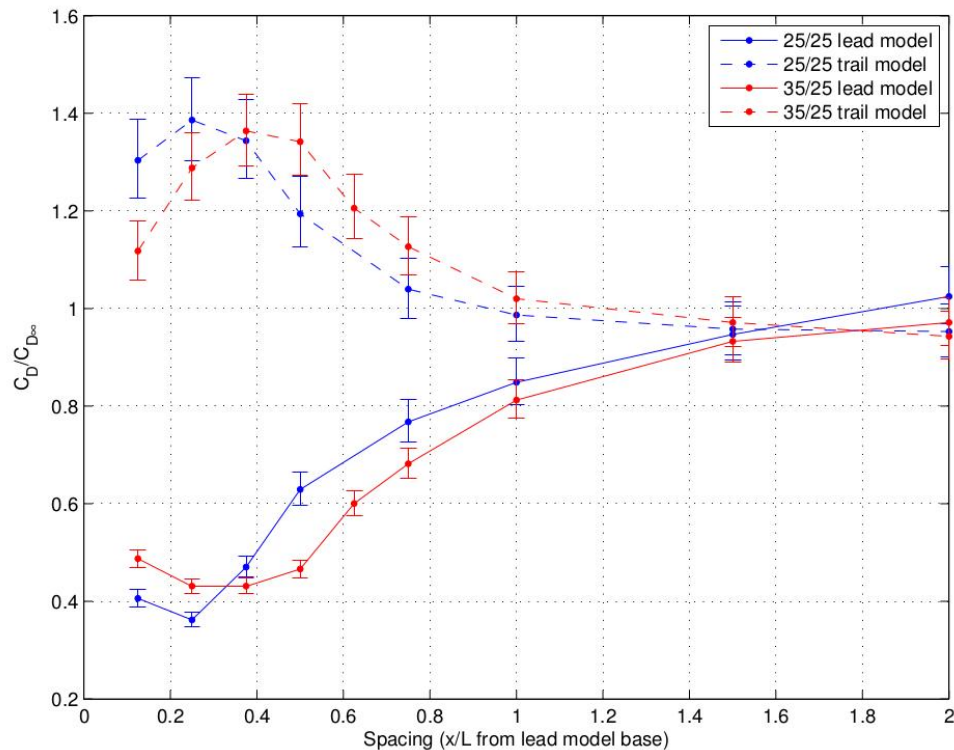
Figure 2.7: Normalized drag force for lead and trail model using Ahmed bodies[4]

The net drag of the system was always reducing with closer spacing, i.e., the lead model drag reduction was higher in magnitude than the drag increase of the trail model. Paglierella attributed this to the impingement of the wake off the lead model on the rear model surface, thus raising the stagnation point at the front of the rear model. The presence of the trailing model inhibited the development of vortices off the rear of the lead model. This impedence of the low velocity flow in the wake of the lead model caused an increase in pressure in the space between them although

having a very insignificant influence on the wake of the trail model. This explains the change in drag for both the models. He concluded that vortex interaction in the inter-vehicle spacing is the reason for drag penalties at a spacing less than 1L. Figure 2.7 shows the drag trends as presented in Paglierella's dissertation.

2.4 Overset Mesh

The overset-grid technique has been in use since 1988 when it was use in NASA simulations. The first overset grid was very difficult to generate eventhough it had less than a million cells due to the lack of computational power. Overset mesh has been developed since then and several software packages now have the ability to easily generate overset grids. The major advantages of the method are as follows:

- Mulitple components can be meshed independently and can be connected later using interpolation methods.

- A much higher local refinement can be achieved wherever necessary.

- Transient simulations were components move can be easily simulated as these independent meshes can be moved as rigid bodies and the solution can be integrated into the overall solution at each time step.

A few limitations are applied while using Overset grids:

1. The Overlap Region - cells in overset and the background in this region has to be of the same order of magnitude

2. While simulating motion, Movement has to be limited to 1 cell per time-step

3. Domain connectivity has to be done where the relation/interaction between overset and the background region or between multiple overset regions is defined and the method of hole cutting operation has to be defined.

Modern software packages takes care of all these difficulties with minimal user input.

CHAPTER 3: TURBULENCE MODELING

3.1   Turbulence and its importance

As long as the scales are small enough and the velocities are low enough, flows are controlled by viscous diffusion of vorticity and momentum. It is termed as laminar and the equations of motion have a steady solution. At larger Reynolds number though, inertial forces overcome viscous forces - unsteadiness and three-dimensional nature is added to the flow. Turbulence in fluid motion is characterized as random, three-dimensional and chaotic. Vorticity generation and its stretching is the root of turbulence and turbulence, if it is present, usually dominates all other flow phenomena. As engineers, or anyone trained in physics for that matter, we try to see physical phenomena as equations and try to solve them. But because of the nature of the turbulence, there is an ambiguity around the mechanics behind it. The understanding of non-linear dynamical systems, their equations and the birth of Chaos Theory play a major role in understanding turbulence.

Researchers now believe the solutions of the fluid mechanical equations to be deterministic by their boundary and initial conditions. Statistical techniques are sought owing to the chaotic and random nature of turbulence. Even with the advances in understanding over the past few decades, together with the advent of large scale computational and experimental capabilities, satisfactory understanding of turbulence presents one of the great remaining fundamental challenges to scientists and engineers as most real world flows are turbulent.

The first step in understanding turbulence would be to represent it mathematically and then solving it. Turbulence modeling is the construction and the use of mathematical models to predict the nature and effects of turbulence in fluid flows. The

work of Reynolds (1985), Boussinesq (1877) and Prandtl (1925) are major milestones that serve as the origin of turbulence modeling[32]. The models that are relevant and were used for this study will be discussed in the following sections.

3.2   Direct Numerical Simulation (DNS)

The Navier-Stokes equations are the basic governing equations for viscous Newtonian fluids. It is a vector equation, also called the conservation of momentum equation, derived from applying Newton's second law of motion to a fluid element. It is supplemented by the mass conservation equation, also called continuity equation. Equations 3.1 and 3.2 represent the conservation equations for mass and momentum respectively. Considering the low mach numbers experienced during on-road situations, the incompressible form of the equation is considered for this study.

$$\frac{\partial u_i}{\partial x_i} = 0 \tag{3.1}$$

$$\frac{\partial u_i}{\partial t} + u_j \frac{\partial u_i}{\partial x_j} = -\frac{1}{\rho}\frac{\partial p}{\partial x_i} + \frac{\partial \tau_{ij}}{\partial x_j} \tag{3.2}$$

$$\tau_{ij} = 2\mu s_{ij} \tag{3.3}$$

$$s_{ij} = \frac{1}{2}\left(\frac{\partial u_i}{\partial x_j} + \frac{\partial u_j}{\partial x_i}\right) \tag{3.4}$$

The Navier-Stokes equations, although being simple, describe the complex and diverse fluid flows accurately and in complete detail. However, this is the downside of the equations as well. The N-S equations describe every detail of the turbulent velocity field from the largest to the smallest scales. The amount of information in these fields is overwhelming that we need statistical methods to solve them.

Direct numerical simulation (DNS) handles a direct approach in solving the N-S equations, where all scales of motions are resolved, from Kolmogorov micro-scales to the characteristic scales. Although it was infeasible until the 1970s, conceptually it is the simplest approach available and it is unrivaled when it comes to accuracy of the solution. Nonetheless, the computational cost is extremely high. It is so high that a full-scale DrivAer model at speeds of 80mph would require a near body mesh size of about 264 trillion cells and would require 30 thousand time steps to simulate 1s of real time to resolve the scales[33]. Thus, DNS is intractable for real-world problems and can only be used as a powerful research tool to understand turbulent flows at moderate Reynolds numbers. Several DNS studies have been conducted on wall-bounded flows, at low to moderate Reynolds numbers, to investigate the underlying physical processes involved and have proved extremely valuable in supplementing our knowledge towards understanding turbulence.

3.3   Turbulent-Viscosity Models (RANS models)

Turbulent-Viscosity models are based on modifying the conservative N-S equation using Reynolds averaging and thus solving for it by modeling the additional Reynolds stress term introduced. Reynolds-Averaged Navier Stokes equation is achieved by ensemble averaging the original N-S equations and it is expressed in its conservative form as in Equations 3.5 and 3.6. Here, we describe the turbulent flow statistically in terms of the mean velocity field U(x,t) instead of the velocity field u(x,t) itself.

$$\frac{\partial U_i}{\partial x_i} = 0 \tag{3.5}$$

$$\frac{\partial U_i}{\partial t} + U_j \frac{\partial U_i}{\partial x_j} = -\frac{1}{\rho}\frac{\partial P}{\partial x_i} + \frac{\partial}{\partial x_j}\left(2\mu S_{ij} - \rho\overline{u_i' u_j'}\right) \tag{3.6}$$

This approach in turn adds an unknown term, τ_{ij} which is the specific Reynolds stress tensor - a symmetric tensor, with six independent components. Now, as a re-

sult of Reynolds averaging, there are six additional unknowns without any additional equations. This means that the system is not closed with ten unknowns and only four equations. This is the closure problem. This closure problem is tackled using the turbulent-viscosity hypothesis introduced by Boussinesq in 1877. Based on Boussinesq's approximation, the Reynolds stresses can be calculated based on turbulent kinetic energy k, eddy viscosity ν_t and mean rate of strain as shown in Equation 3.7

$$\overline{u_i' u_j'} = \frac{2}{3} k \delta_{ij} - \nu_t \left(\frac{\partial \overline{U}_i}{\partial x_j} + \frac{\partial \overline{U}_j}{\partial x_i} \right) \tag{3.7}$$

The numerous models that has root based on this hypothesis differ in the way they calculate eddy-viscosity, ν_t. These models can be classified into linear eddy-viscosity models, non-linear eddy-vicosity models and Reynolds Stress Models (RSM) based on the approach to model the above mentioned Reynolds stress term. The linear eddy viscosity models are further classified into one-equation and two-equation models based on the number of transport equations involved. Spallart-Allmaras is one of the most famous one-equation models. Among the two-equation models, k-ϵ[34] and k-ω[35] models are the most widely used. Several modifications have been done to improve performance of these models for a wide range of flow fields and hence has been studied the most. Hence, two-equation models are the most common and widely used and have become industry standard models.

Kolmogorov was the first to propose a two-equation model in which he used a second parameter, the specific dissipation rate, ω, and modeled the differential equation governing its behavior. The k-ϵ model by Jones and Launder[34] and Wilcox's k-ω model[35] are the most popular and both solve velocity scales through turbulent kinetic energy and a second transport equation to solve the turbulence length scale. Both models have shortcomings - k-ϵ performs poorly near the wall because it over-predicts eddy-viscosity near the wall as k tends towards zero while the k-ω model is sensitive to free stream/inlet conditions. These shortcomings were addressed by

Menter[36] when he proposed the Shear Stress Transport version of the k-ω model, employing the best of both the base models of k-ϵ and k-ω. He used a blending function F1 as shown in Equation 3.9 to switch between ω based models near the wall and ϵ based away from it.

From the several models tested for this study; SST k-ω model, SST for short hereinafter, proved superior to the other models. The SST Menter model, in spite of its complexity, struggles to accurately predict separation lengths because of its inability to resolve large scale unsteadiness albeit proving superior in overall predictions when compared to other models tested. The transport equations of the SST model is shown is the following equations.

$$\frac{\partial k}{\partial t} + U_j \frac{\partial k}{\partial x_j} = P - \beta^* k\omega + \frac{\partial}{\partial x_j}\left[(\nu + \sigma_k \nu_t)\frac{\partial k}{\partial x_j}\right] \tag{3.8}$$

$$\frac{\partial \omega}{\partial t} + U_j \frac{\partial \omega}{\partial x_j} = \frac{\gamma}{\nu_t} - \beta^* \omega^2 + \frac{\partial}{\partial x_j}\left[(\nu + \sigma_\omega \nu_t)\frac{\partial \Omega}{\partial x_j}\right] + 2(1 - F_1)\frac{\sigma_{\omega 2}}{\omega}\frac{\partial k}{\partial x_j}\frac{\partial \omega}{\partial x_j} \tag{3.9}$$

$$P = \tau_{ij}\frac{\partial u_i}{\partial x_j} \tag{3.10}$$

$$\tau_{ij} = \mu_t\left(2S_{ij} - \frac{2}{3}\frac{\partial u_k}{\partial x_k}\right) - \frac{2}{3}\rho k\delta_{ij} \tag{3.11}$$

$$\mu_t = \frac{\rho a_1 k}{\max(a_1 \omega, \Omega F_2)} \tag{3.12}$$

The coefficients for the model are calculated from the blending function F_1, such that each coefficient ϕ is given by:

$$\phi = F_1\phi_1 + (1 - F_1)\phi_2 \tag{3.13}$$

The coefficients for the set 1 (ϕ_1) are

$\beta_1 = 0.0750, \quad \sigma_{k1} = 0.85, \quad \sigma_{\omega1} = 0.5, \quad \kappa = 0.41, \quad \gamma_1 = \frac{\beta_1}{\beta^*} - \sigma_{\omega1}\frac{\kappa^2}{\beta^*}$

The coefficients for the set 2 (ϕ_2) are

$\beta_2 = 0.0828, \quad \sigma_{k2} = 1.0, \quad \sigma_{\omega2} = 0.856, \quad \kappa = 0.41, \quad \gamma_2 = \frac{\beta_2}{\beta^*} - \sigma_{\omega2}\frac{\kappa^2}{\beta^*}$

for both set 1 and set 2

$\beta^* = 0.09 , \quad \alpha = 1$

These are called the closure coefficients. These were used to create algebraic expressions with known turbulence and mean-flow properties to replace the unknown correlations involved in the RANS modeling as it was based mainly on dimensional analysis. The values for these coefficients were set by observations and agreement to known canonical flow properties. Hence, it is not surprising that RANS often fail to predict flow fields involving massive flow separations with complex flow structures. Therefore, the study intends to test several simulation strategies and explore the possibility of improving the prediction veracity of the SST model in transient cases involving multiple bodies.

3.4   Detached Eddy Simulation (DES)

Detached Eddy Simulation was introduced by Spalart et al., in 1997 as a cost-effective method of simulating turbulence. The principle behind DES is that larger eddies are treated using the conventional wall-resolved Large Eddy Simulation (LES) whereas the thin shear layers and the boundary layers are treated using RANS approach. This greatly reduced computational requirement as RANS, unlike LES, does not require very fine isotropic cells in the boundary layer. In each cell, the effective

turbulent length scale, l_t ,given in Equation 3.14 and the local finite-difference cell size, l_{LES}, are computed. Wherever $l_t < l_{LES}$, RANS is implemented [Wilcox].

$$l_t = \sqrt{k}/\omega \tag{3.14}$$

$$l_{LES} = C_{DES}\Delta_{IDDES} \tag{3.15}$$

where C_{DES} is a constant and Δ_{IDDES} is the filter width based on local mesh resolution.

Large Eddy Simulation (LES) was proposed based on the argument that small-scale turbulence contribution to Reynolds stresses is much weaker when compared to largest eddies. Thus, LES segregates the wide turbulent scales into largest scales that will be computed and the sub-grid scales (SGS) which will be modeled. This means that the grids need not be as fine as for a DNS study and thus, it is possible to achieve higher Reynolds number with LES than with DNS at less computational cost. The primary difference between DNS and LES comes from the concept of filtering. The scales smaller than the grid size are filtered out and modeled. There are many types of filters that can be used. Similar to the RANS models, there is an extra term added in the momentum equation after filtering and this extra term has to be modeled. The choice of filter type is very influential in LES solutions.

The IDDES was proposed as an improvement over the DES and DDES model, correcting for the overestimation of dissipation due to premature switch from RANS to LES. The specific dissipation rate and the blending function in the RANS-SST is modified for IDDES-SST as

$$\tilde{\omega} = \frac{\sqrt{k}}{l_{HYBRID}\beta^* f_{\beta^*}} \tag{3.16}$$

where, f_{β^*} is the free-shear modification factor and l_{HYBRID} is the hybrid length

scale determined based on the effective length scale and the local grid size using a blending function and an elevating function.

$$C_{DES} = C_{DES,k-\omega}F_1 + C_{DES,k-\epsilon}(1 - F_1) \tag{3.17}$$

where $C_{DES,k-\epsilon} = 0.61$ $\quad and \quad$ $C_{DES,k-\omega} = 0.78$.

CHAPTER 4: NUMERICAL SETUP

This chapter elucidates the details related to the numerical setup for each simulation carried out and the finite volume grids that has been used in the study. The setup was refined through the course of the work based on the knowledge gathered with every successive test case. Nonetheless, a few settings were maintained throughout the study. The commercial finite volume CFD code, STAR-CCM+ is being used for the study. The initial test cases to study the influence of grid size and turbulence models were studied using STAR-CCM+ v11.04 and the rest used v12.06 of the same. All the simulations were run using a segregated incompressible unstructured solver utilizing SIMPLE algorithm. An Algebraic Multi-grid (AMG) linear solver using a combination of V cycle and a flex cycle was used for the momentum equations and turbulent quantities. Temporal discretization is achieved using a first-order Euler implicit method and hybrid second-order BCD was used for spatial discretization. A two-layer all y^+ wall-function approach was used in conjunction with all the turbulence models tested. The reason for using this wall treatment is to make sure we get reasonable results even where we are not able to maintain a fine enough mesh because of the complexity and difficulties with the sharp edges and intricate shapes of both the test geometries. The wall treatment relies on wall function wherever the mesh is coarse. A CFL number independence study was carried out and all the URANS simulations were run with a CFL number of $\approx$4. The IDDES simulations employed a CFL number of $\approx$1. The time-steps are shown in table4.1 for both cases.

Table 4.1: Time-step used for each case in seconds.

	Cube	DrivAer
Reynolds Number	$22.5 \text{x} 10^3$	$4870 \text{x} 10^3$
URANS	$1 \text{x} 10^{-3}$	NA
IDDES	$0.25 \text{x} 10^{-3}$	$0.15 \text{x} 10^{-3}$

The following sections describe briefly the test cases carried out to make sure that the setup is free from the influence of grid settings and other physics settings. These studies are carried out using the surface-mounted cube setup as it was computationally less expensive and had a shorter turn around time. The information accumulated from these studies were then applied to the computational setup with the DrivAer reference geometry, which is detailed in the last section of this chapter.

4.1   Surface-mounted Cube

CFD usually requires a compromise between accuracy and cost-efficiency. This must be taken into serious notice because during grid selection we might not choose a finer grid even if it gives us a marginally better result based on the computational requirement it stacks up. RANS approach is not as bad as it has been labeled in predicting the overall aerodynamic characteristics if it is carefully crafted. Although we are using wall functions in our modeling approach, we intend to keep the wall y^+ below 1 in case of the surface-mounted block and at least 5 in case of the DrivAer reference geometry as shown in figure 4.1. This was achieved by using anisotropic prism layer cells near the no-slip surfaces of the domain. The bump in the DrivAer case is owing to the complexity of the geometry. The prism layer settings for the setup with the surface-mounted cube and the fastback DrivAer geometry are shown in table 4.2. In the table, y_1 represents te first layer thickness and T represents the total thickness.

Table 4.2: Prism layer settings used for the studies

Surface	y_1 (in mm)	No. of layers	T (in mm)
Cube - Surface and Ground	0.0165	7	2.0
DrivAer - Body surfaces	0.0125	9	6
DrivAer - Underbody	0.025	8	6
DrivAer - Wheels and Exhaust system	0.025	7	3
DrivAer - Ground	0.1	7	12
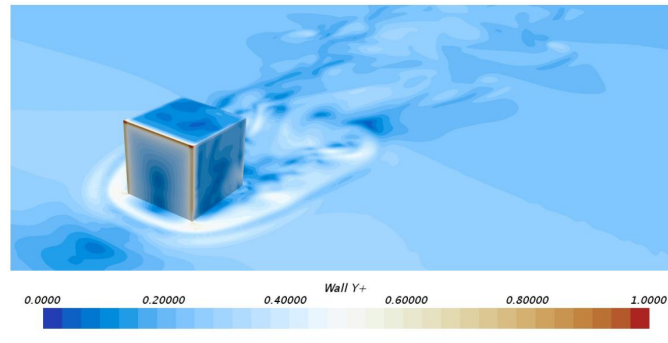
(a) Surface-mounted cube
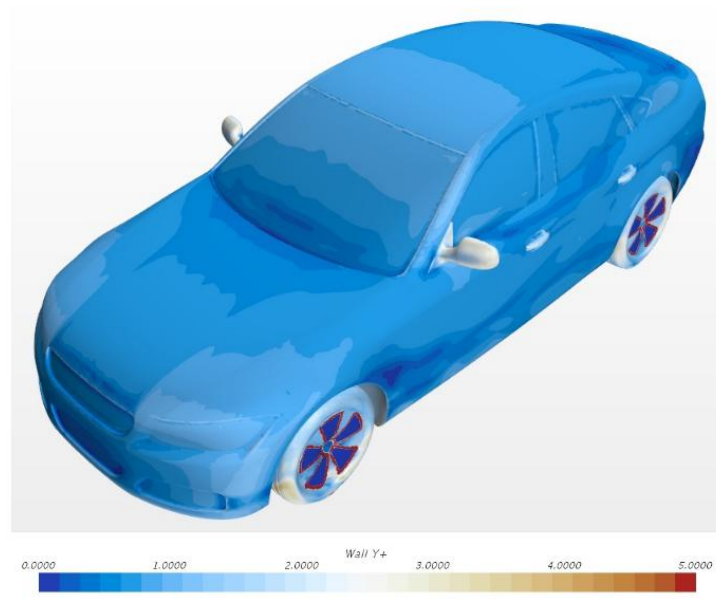
(b) DrivAer

Figure 4.1: Scalar scenes showing wall y^+ values for each case

The computational domain was chosen to replicate a free flow test environment with a negligible blockage interference. A 40mm(h) cube is used in order to replicate the work of Martinuzzi and Havel[25, 24]. The computational domain was split into two sections: a front channel-section having a slip wall boundary condition on the ground surface and a rear test-section. This was used to make sure the flow is fully developed when it reaches the test-section. The cube was mounted 2L from the the junction of slip and 'no-slip' domains to make sure we attain the same boundary layer thickness when it reaches the block as used by Martinuzzi and Havel. A velocity inlet was defined with a velocity of 8.8m/s which gives a Reynolds number of $\approx$22500 . The lateral boundaries and the top were specified as 'Symmetry planes'. The cube surface and the test section ground were defined as 'no-slip' walls. The outlet was placed far enough from the test object to avoid any pressure reflections.

Then, the base size was varied to reach mesh independence. Base size is the smallest surface size used in the grid. This parameter mainly influences the viscous drag prediction and the evaluation of other gradients surrounding the surfaces. Several base sizes from 4mm to 1mm were tested and their influence on force predictions were studied. It is understood that drag prediction has not been affected below the mesh base size of 2mm, which is 1.3 times the "Taylor microscale". The near wall mesh and prsim layers are shown in figure 4.2. The Taylor microscale approximation equation estimated by Kuczaj et al. used for a priori estimate of Taylor microscale length is shown in equation 4.1

$$\lambda = \sqrt{15}\frac{1}{\sqrt{A_1}}\frac{1}{\sqrt{Re}}L \qquad (4.1)$$
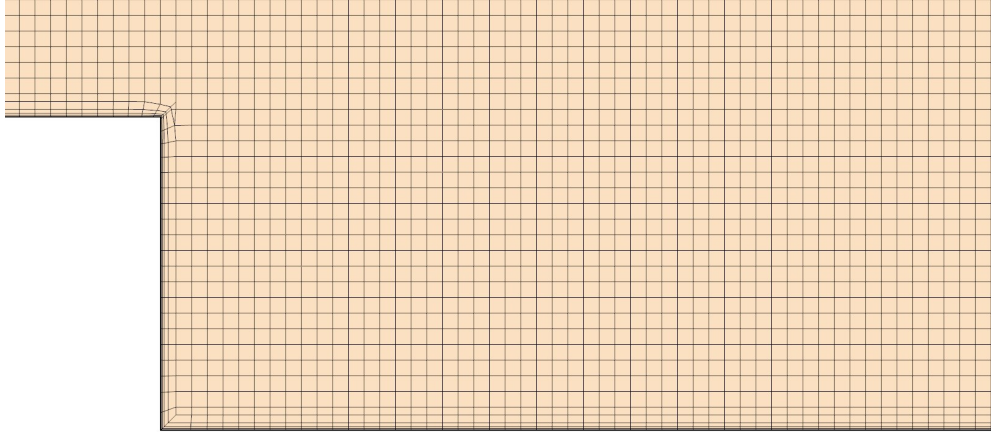
Figure 4.2: Grid representation near the cube surface

A drag prediction change of 0.1% was observed when going down from 2mm to 1mm while the total cell size was quadrupled. Thus, the mesh refinement from 2mm to 1mm require almost 4 times the computational resources whereas there is no substantial gain in accuracy.

Similarly, several volume sources with varying sizes, increasing both laterally and in the normal direction, were tested. The final mesh consists of three volume sources, as shown in figures 4.3 and 4.4, with 10mm, 60mm and 80mm from the surface of the cube in lateral and vertical directions. An anisotropic mesh with a cell growth ratio of not more than 2 in all the directions were used. Volume sources, excluding the inner most, were extended from inlet to the outlet as shown in figures below to make sure we have a fully developed flow reaching the block as well as keeping the tandem case study in mind. Wake refinement study was done with the inner most volume source and a stream-wise length of 160mm(4h) behind the cube was finalized.

The final discretized domain consists of 5.7 million unstructured cells, generated using the trim-mesher in STAR-CCM+. The setup with tandem cubes came up to 7 million cells.
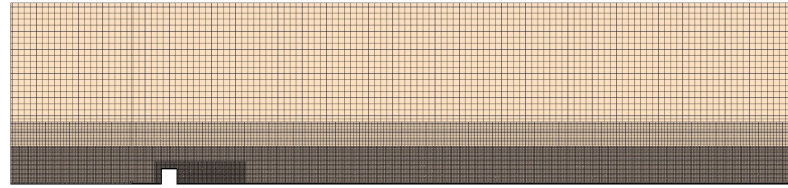
(a) Distant view
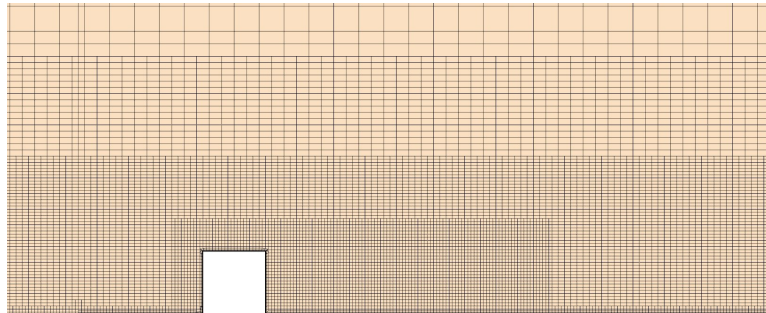
(b) Close view

Figure 4.3: Mesh slices of domain for the surface-mounted cube at Y=0L plane
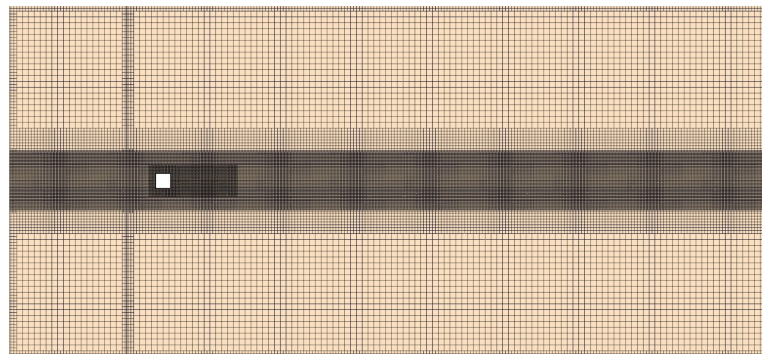
(a) Distant view
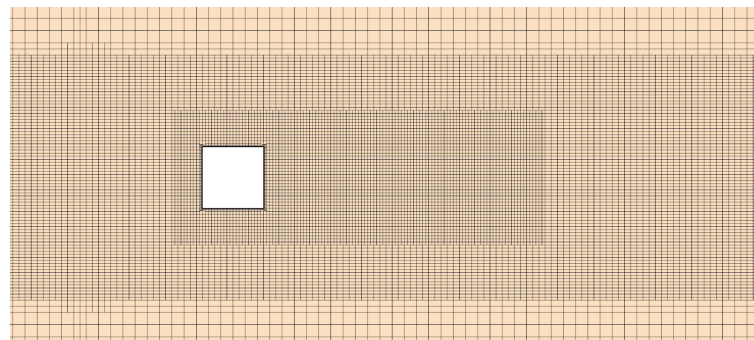
(b) Close view

Figure 4.4: Mesh slices of domain for the surface-mounted cube at Z=0L plane
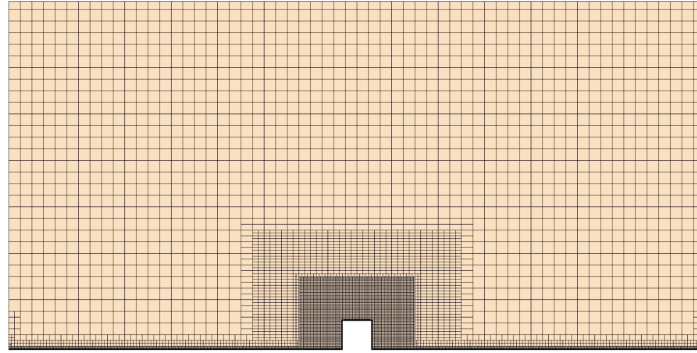
(a) Distant view
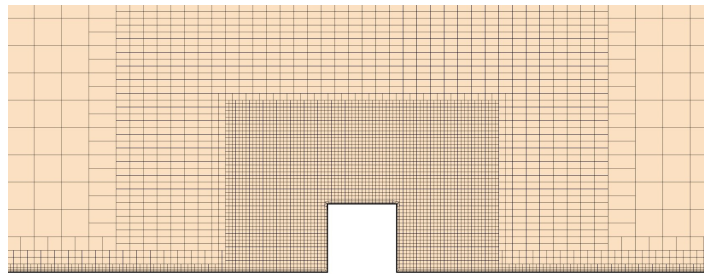
(b) Close view

Figure 4.5: Mesh slices of domain for the surface-mounted cube at X=0L plane

Three different RANS models were studied using the surface-mounted cube setup to choose the model which is able to reproduce most of the flow features with at-most accuracy. The turbulence models tested were Realizable k-ϵ(RKE), SST Menter k-ω(SST) and ν^2-f(V2F) models. The isosurfaces of flow features predicted by these models are presented in figure 4.6. As seen in the figure, although RKE model has better agreement with the reattachment length behind the cube, it fails to reproduce the horse-shoe vortex system as predicted by other experimental and DNS studies. V2F model has the worst prediction of the reattachment length in spite of being able to predict the horse-shoe system with good accuracy. The author chose the SST model considering the data available in the ability of improving the SST model and carried on tests to explore the possibilities of improving the prediction veracity of the model.
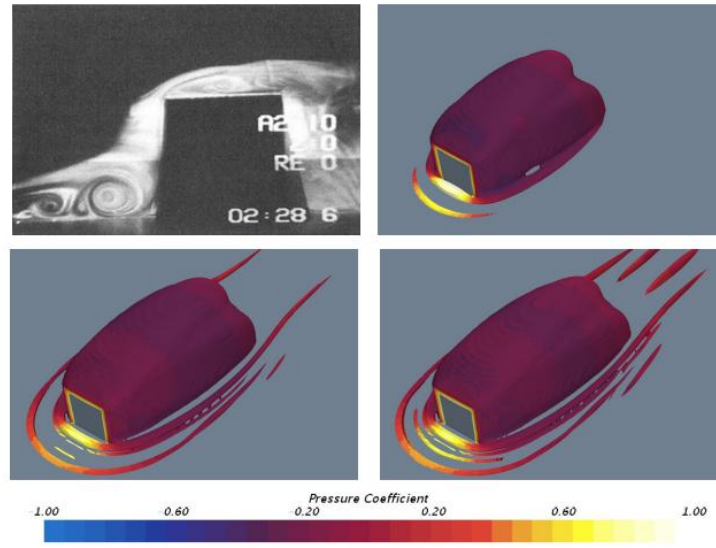
Figure 4.6: Isosurfaces of Q* showing flow predictions of different models: RKE(top-right), SST(bottom-left), V2F(bottom-right)

RANS turbulence models have unknown closure coefficients in their transport equations as these equations are developed based on dimensional analysis. The k-ω model has six of these closure coefficients, viz., α, β_o, β^*, σ, σ_* and σ_{do}. The closure coefficients influence the respective terms they are involved with in the transport equations. Hence, they impact the prediction of production, dissipation, diffusion and cross-diffusion of turbulent quantities. The default values set for the SST models are based on canonical flows and the properties of turbulence observed from these flows. So, it is highly unlikely that the model would predict the automotive flows as well due to the higher magnitude of separations and reattachments happening over an automotive surface. The author however, does not try to modify all the coefficients. Three selected coefficients were modified and a combination of the better values were chosen and tested based on their individual influence on the flow predictions. For this, we focus on the changes in prediction of the primary recirculation region as it is directly related to the turbulent prediction of the shear layers separating from the leading edge of the cube.

Nonetheless, one should be aware of the limitations in modifying these coefficients

as it might render the flow unphysical. There are some limitations and conditions to be met so that the equations satisfy the physics of the flow. For example, the von-karmann constant κ, which is a function of C_{ϵ_1} and C_{ϵ_2}, should not exceed a value of 0.41. κ can be calculated using the following equation:

$$\kappa^2 = \sigma_\epsilon C_\mu^{\frac{1}{2}} (C_{\epsilon 2} - C_{\epsilon 1}) \tag{4.2}$$

The modifications made in this work obey these limitations strictly and only three coefficients, β^*, $\sigma_{\omega 1}$, $\sigma_{\omega 2}$,have been modified.

Table 4.3: Influence of β^* on the prediction of primary recirculation region length and C_D

Case	1	2	3
β^*	0.07	0.09	0.1125
X_R in cube lengths	4.95	5.3	6.0

Table 4.4: Influence of $\sigma_{\omega 1}$ on the prediction of primary recirculation region length and C_D

Case	1	2	3	4	5
$\sigma_{\omega 1}$	0.4	0.5	0.55	0.65	1.1
X_R n cube lengths	5.4	5.3	5.3	5.1	4.6

Table 4.5: Influence of $\sigma_{\omega 2}$ on the prediction of primary recirculation region length and C_D

Case	1	2	3	4	5
$\sigma_{\omega 2}$	0.8	0.856	1.05	1.1	1.7
X_R in cube lengths	5.5	5.3	4.6	4.5	4.2

In the above tables, we see how each coefficient affect the prediction of reattachment point in the wake of the cube. The experimental value for X_R is 1.7. The individual

modifications improve the prediction of this reattachment point as we see a clear trend in each of the coefficient. Hence we choose the best possible combination and test the combination's effect on the resulting recirculation region length prediction. The final combination chosen for the study was β^*=0.07, $\sigma_{\omega 1}$=1.1 and $\sigma_{\omega 2}$=1.7. Out of these three coefficients, $\sigma_{\omega 2}$ seem to have the highest influence on the flow. Higher values of β^* were not tested as the flow started to become unphysical. The reattachment length predicted by this combination of coefficients was 2.8L which is a significant improvement over the default prediction which was 5.3L. The flow field was analyzed for any abnormalities that might have been caused by these modifications and none were found. Henceforth, the model using these combination of coefficients will be addressed as the modified model.

4.2   DrivAer

For this study, a 40% scaled model of the fastback type DrivAer geometry, as shown in figure 4.7, was used with a detailed underbody, mirrors and wheels.
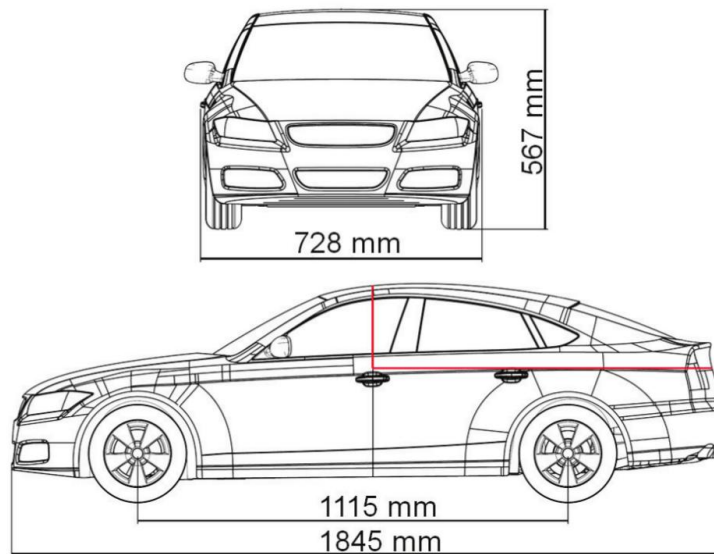
Figure 4.7: Main Dimensions of the 1:2.5 DrivAer Model

The domain was constructed similar to the cube setup, keeping the blockage ratio negligible. The domain was 46Lx26Wx12H in stream-wise, cross stream-wise and

wall normal directions as shown in figure.
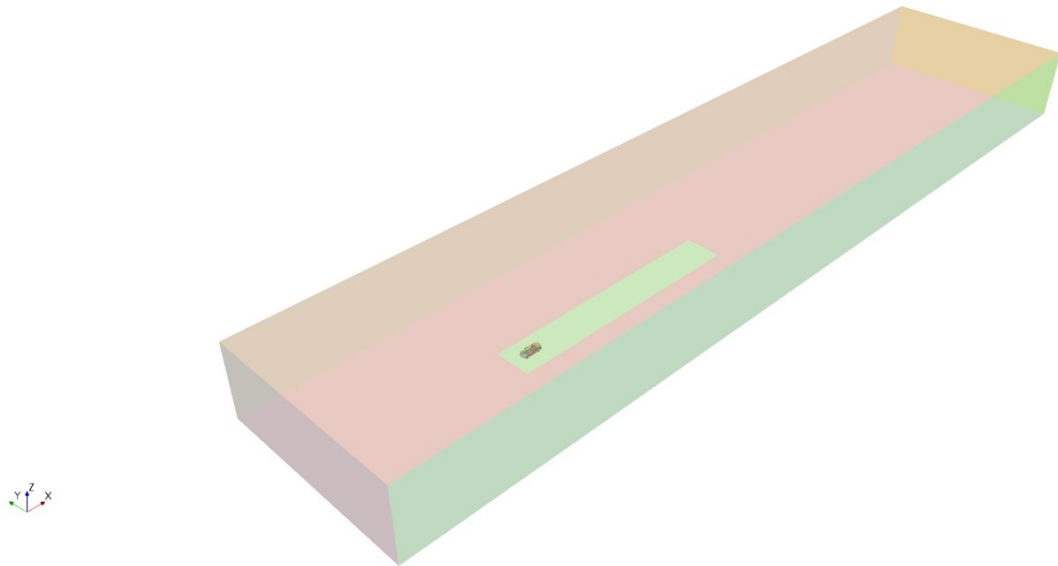
Figure 4.8: Computational domain used for simulating the DrivAer reference geometry

Unlike the cube, DrivAer geometry cannot be used directly as is. Several geometric simplifications has to be made as the geometry is complex with numerous intricate shapes to be used in a CFD study directly. Hence, the original CAD files were imported into ANSA and simplifications were done. A water tight mesh was also created in ANSA before importing the geometry back to STAR-CCM+ where it was re-meshed to the required base size, which was fixed at 6mm based on the information gathered from earlier studies on the cube. Figure 4.9 show the mesh generated using ANSA compared to the re-meshed surface in STAR-CCM+. The tire contact patch was simplified in order to avoid skewed cells around the tire-ground junction.

(a) Isometric View

(b) Nose

(c) Underbody

Figure 4.9: Comparison of surface mesh from ANSA(fine) and surface mesh after remeshing(coarse) in STAR-CCM+

The boundary conditions are similar to that of the cube setup with an inlet velocity of 40m/s which amounts to a Reynolds number of 4870×10^3 based on the inlet velocity and a reference length of 1.85m. To preserve the mesh size, a no-slip patch(the green patch on the ground as seen in figure 4.8) was used instead of a complete section as in the case of the cubes. This patch extended half car length in front of the lead car and 10.5L behind its base. The width was 2.5W on either side of the car. This no-slip ground was given a tangential velocity of 40m/s. The pumping effect of the wheels were reproduced using Moving Reference Frames(MRF). The tires and rest of the rims were given a local rotation rate. The volumes sources were adjusted based on the considerations such as the size of the DrivAer wake, available resources and computed Taylor microscales. On account of achieving a good balance between accuracy and computational cost, the volume sources were constructed to follow the external shape of the vehicle. The volume sources were made as shells following the car's shape and expanded in normal and lateral directions with a boxed wake refinement to resolve the wake. The first layer of refinement extended to a distance to compose 20 layers of the 'base' size cells in wall normal and lateral directions. The layers of refinement after the first had 15 layers of cells before transitioning to the next cell size. The wake refinement of the the innermost volume source extended 0.5 car lengths behind the vehicle base, the second extended 1L behind the case, the next one was 3L and the last one, which acted as the overlap region for the overset and background, was the longest and extended over 8L behind the base of the lead car. The final mesh had a total of 27.7 million unstructured trim-cells for the isolated case and 54.2 million cells for the platooning case. The final mesh representation is shown in figures below.
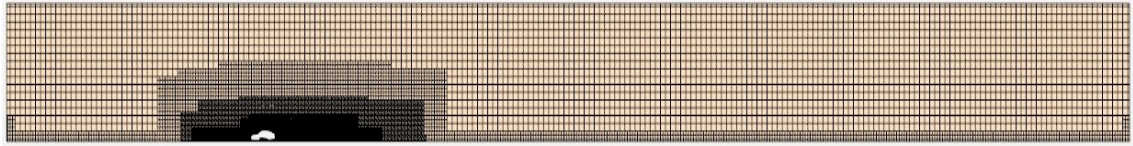
(a) Distant view
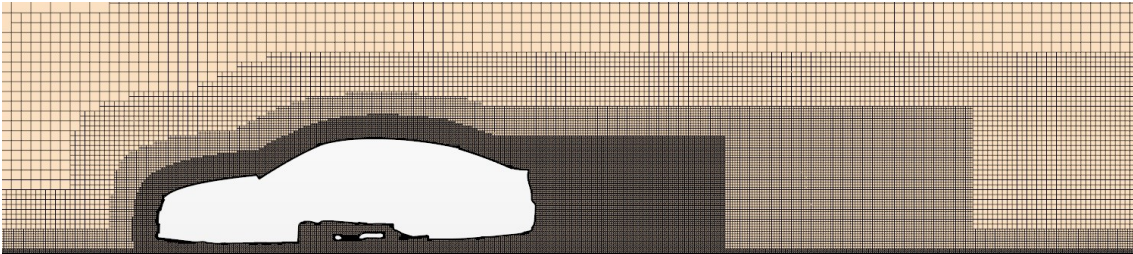
(b) Close view

Figure 4.10: Mesh slices of domain for the DrivAer model at Y=0L plane
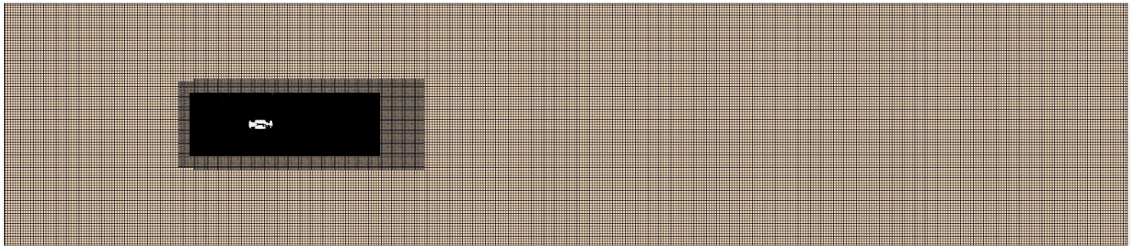
(a) Distant view
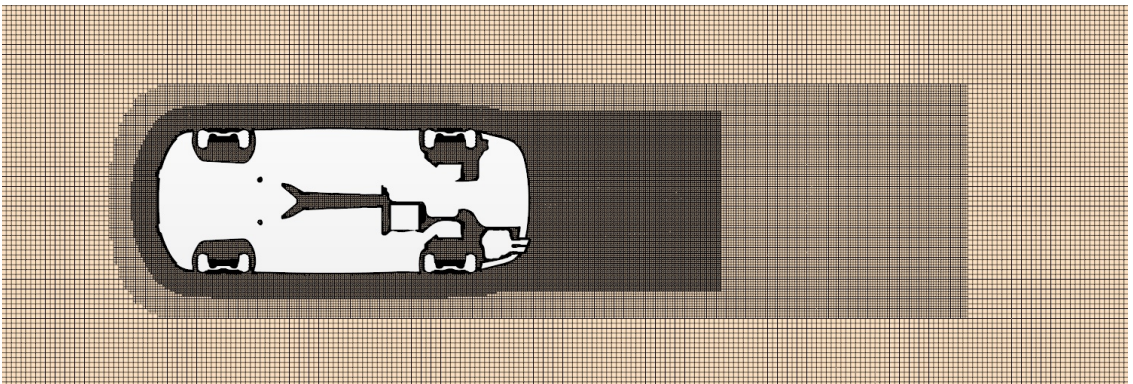
(b) Close view

Figure 4.11: Mesh slices of domain for the DrivAer model at Z=0L plane
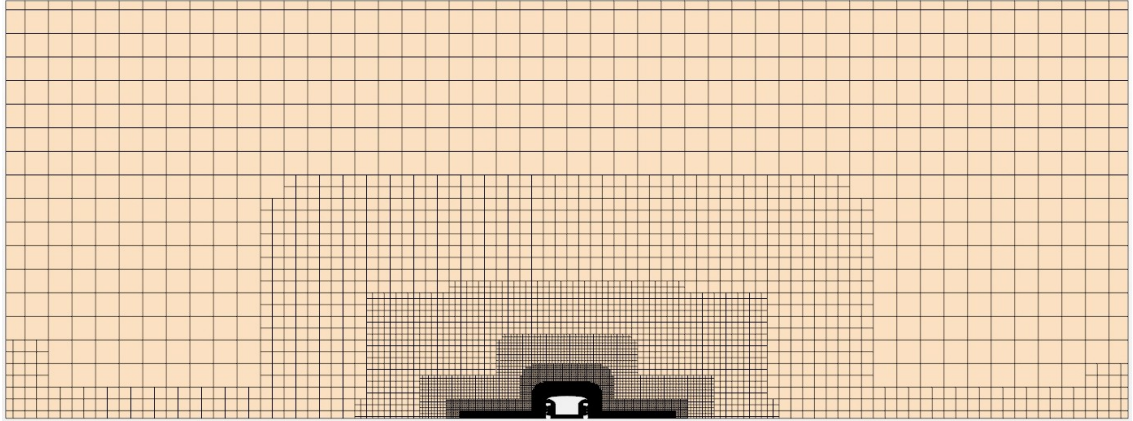
(a) Distant view
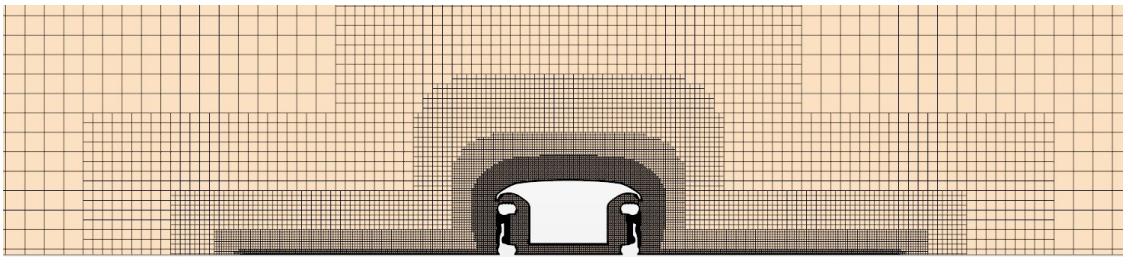
(b) Close view

Figure 4.12: Mesh slices of domain for the DrivAer model at X=0L plane
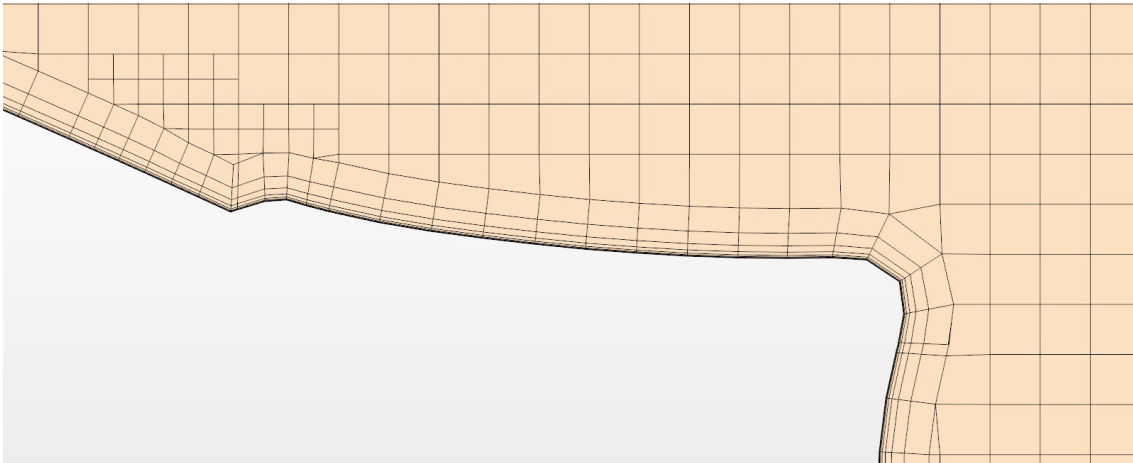
Figure 4.13: Detail slices of mesh over the rear glass and deck-lid junction at Y=0L plane

CHAPTER 5: TANDEM BLUFF BODIES

This chapter focuses on the influence on multiple body interference using surface-mounted cubes. The study is done using the quasi-steady approach. We chose the cube because of its simplified shape and thus the reduced computational ask to test multiple cases until we come up with a final simulation method. Additionally, there are numerous research data available, both experimental and DNS, to validate and correlate our results. Unsteady RANS simulations were run for 100 large eddy turnover time(LETOTs) and averaged over 30 of the same while IDDES simulations were run for 360 LETOTs and averaged over 270 LETOTs to get the mean flow fields. The averaging period is critical in case of IDDES as prolonged averaging over at least 200LETOTs is necessary in the case of surface-mounted cubes to get a reasonable mean flow.

5.0.1   Model Validation

Before simulating the tandem cases, it is vital to perform a validation study making sure that the setup is able to replicate flow features observed in an experimental study or a DNS work. In this case, multiple studies are used as references as the deconstruction of the flow around a surface-mounted cube stretches over years of multiple research work. The Reynolds number of these work vary between 5610 to 40,000 based on cube height. The results from these work have been used in spite of the Reynolds number swing because Castro et al. found that the global flow characteristics(viz., the location of horse-shoe legs, the size of the wake and the like) depend only on the upstream conditions especially the thickness of the boundary layer[20]. Even though the setup using default SST model previously mentioned was

able to reproduce the horse-shoe system in front of the cube, it had shortcomings such as the over-prediction of the wake length. The modified SST however, was able to perform better, especially with the combination of the coefficients. The length of the recirculation region is of primary interest as it has to be made sure that the wake is sufficiently resolved in order to bring in the trailing body. If not, the setup would fail to predict the flow features and body forces of the trailing body with acceptable accuracy.

Both URANS and IDDES were able to predict the upstream recirculation although there were differences in the strength of the horse-shoe vortex. This will have an impact on the prediction of the wake flow. Castro in his work[20] highlights that the vortex promotes turbulent mixing near the base of the body and hence, the larger the vortex the greater the amount of base pressure relieved. This explains the difference in the drag force prediction between URANS and IDDES. There is not much data on drag force at this particular Reynolds number and so, the final setup would be validated for drag prediction with a Reynolds number used by Curley et al.[17] in their work.
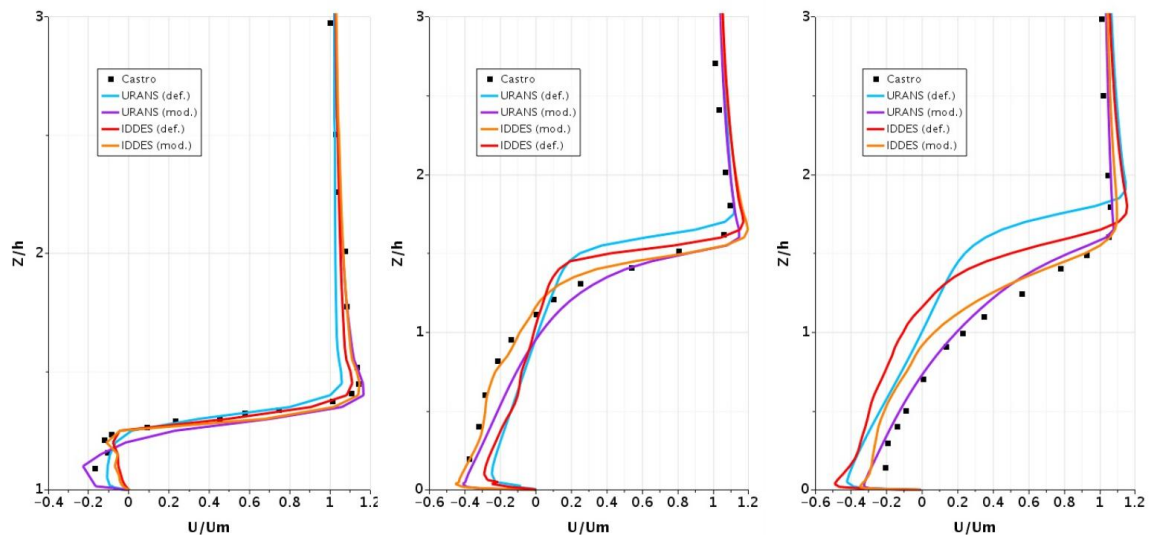
Figure 5.1: Streamwise mean velocity variations in the symmetry plane at x/h=0(left), x/h=1.0(middle) and x/h=2.0(right)

Figure 5.1 shows the variations of mean x-velocity at different locations in the stream-wise direction along the vertical plane of symmetry. It is clear that the models perform noticeably better when the coefficients are modified. The clear problem with the default models is that they over-predict the shear layers separating from the leading top edge of the cube. When looked at the velocity variations over the cube and in the near wake region, URANS perform slightly better than IDDES. This might be due to the fact that IDDES uses URANS to model the flow near the surface and the transition to LES is grid based as discussed in the Turbulence modeling section. This might have caused some abrupt transitions and hence the defect.
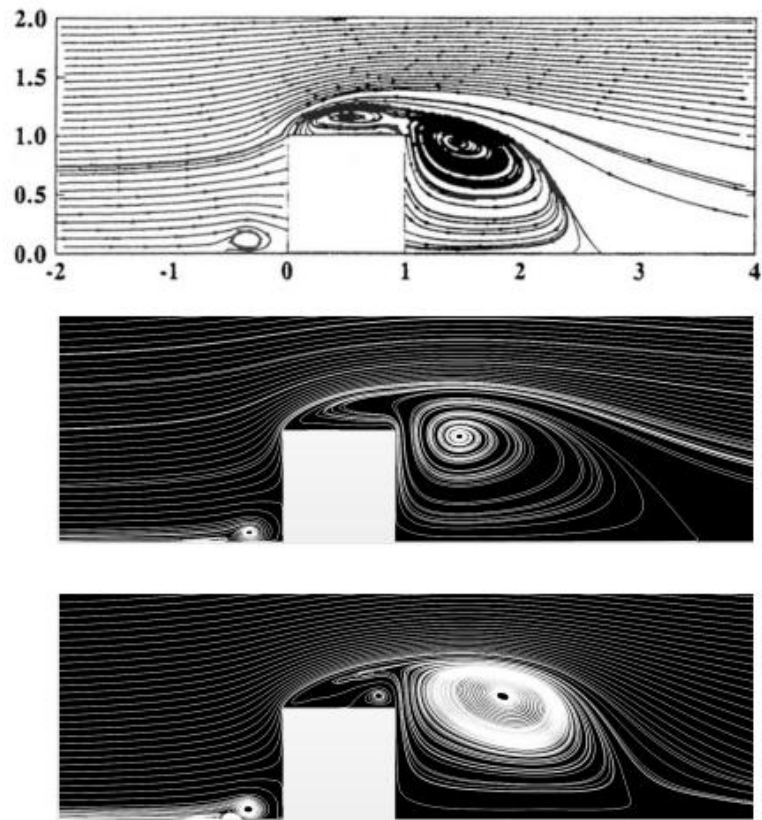
Figure 5.2: Streamlines on the symmetry plane: Experimental[16](top), modified URANS(middle) and modified IDDES(bottom)

Flow visualized in Figures 5.2 and 5.3 contains streamlines of the time-averaged velocity field. In both the models, an upstream HS system exists, together with a

primary recirculation region downstream of the cube. The vortex core is slightly higher and father away in case of the IDDES calculations while the broad features of the flow are in remarkable agreement. The length of the primary recirculation zone as calculated by the models were higher than the experiment at around 2.5h where the experimental value was 1.7h. This is due to the change in blockage ratio of the domains used.
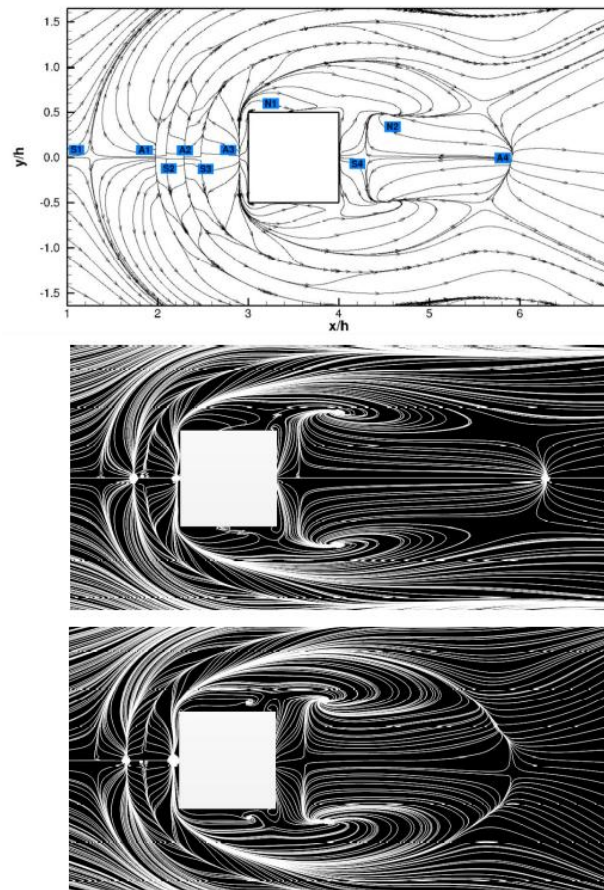
Figure 5.3: Streamlines on the plane Z/h=0.003: DNS[17](top), modified URANS(middle) and modified IDDES(bottom)

Most of the experiments were carried in a channel like domain with a high blockage ratio whereas this study has a negligible blockage ratio in order to simulate a free-flow test environment. Castro has documented the impact of blockage ratio in his work[20]. Castro documented that the tunnel walls "constrict" the wake and the

effect increased with increase in blockage ratio. There will be considerable differences in pressure distribution and hence the drag as well. This is a reason to not make exact quantitative comparison but rather to look at the overall flow features and the trends in the profiles.

In figure 5.3 it is clearly seen that there is a difference in the prediction of the recirculation zone length and also, the number of horse-shoe vortices predicted by the current data are less than what was documented by Curley[17]. The current data predicted only three distinct horse-shoe vortices while one of them was weaker in the URANS predictions.
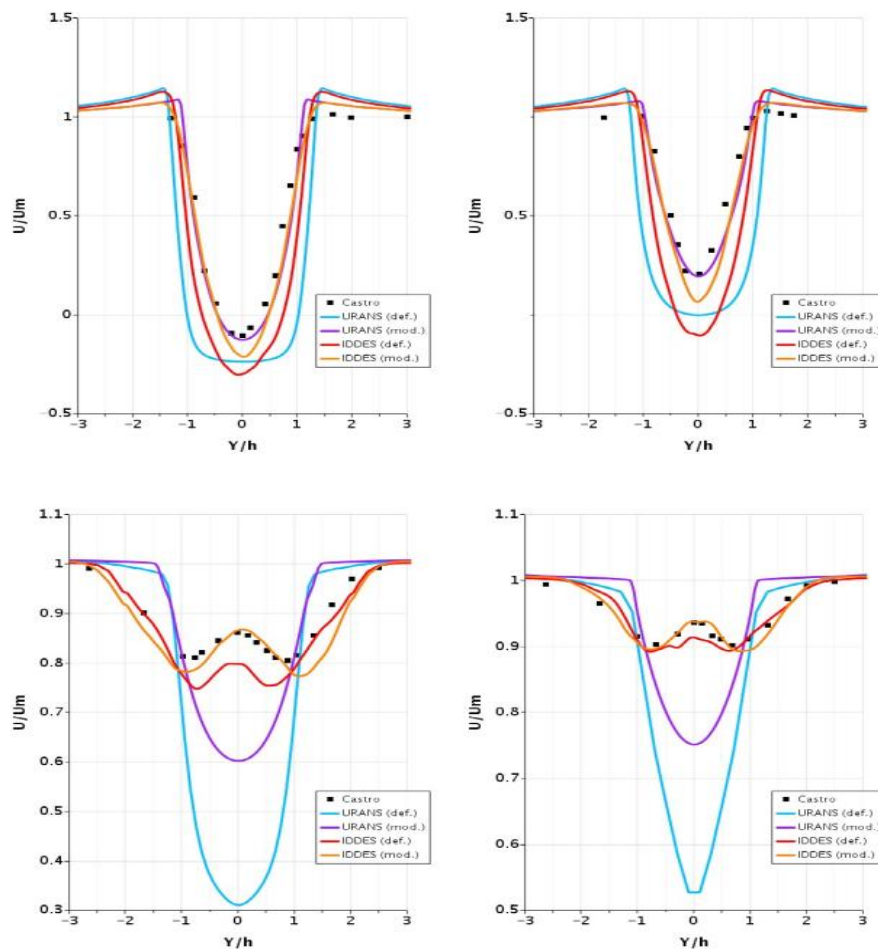
Figure 5.4: Spanwise mean velocity variations in the symmetry plane: top-x/h=2.0[left-z/h=0.5 and right-z/h=1.0], bottom-x/h=6.5[left-z/h=0.5 and right-z/h=1.0]

The IDDES formulation excels in the far wake region where the URANS model completely fails to predict the axial peaks in the velocity variations as seen in figure 5.4. The dips on either side of the peak is due to the horse-shoe vortex extending behind the cube in the wake. In spite of improving the predictions considerably, the modified URANS is unable to resolve the far wake properly. This was documented earlier in Watts' work as well[7]. Watts carried out simulations with two trucks a 1000ft apart. From the velocity scalars(see figure 5.5), it was clear that the URANS model failed to reproduce the wake flow behind the truck and the wake was never fully terminated. This resulted in the wake of the lead truck to have an effect on the trailing truck even at that long of a distance. These discrepancies did not invalidate the results from URANS simulations though, as the values were pretty close to experimental results at close spacings. But, this cannot be applied for our case as watts tested for spacings less than one truck length.

(a) RKE

(b) DES
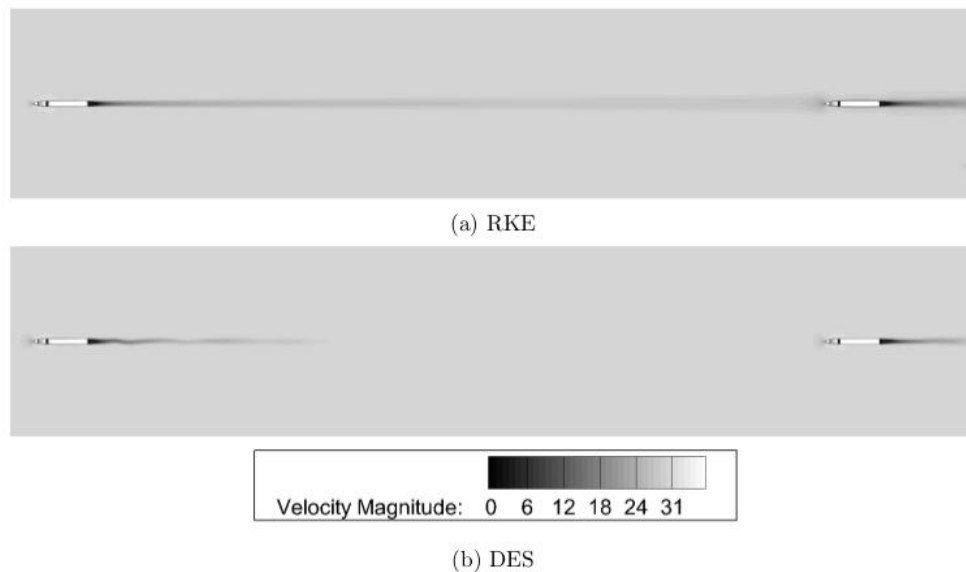
Figure 5.5: Velocity scalars presented by Watts[7]

The reason for this is the inability of RANS models to capture the process of relaminarization. Relaminarization is a process by which a turbulent flow dissipates its energy and returns to a laminar state. This stands as the main reason for the author

to use IDDES for further studies of tandem interferences. A comparison between skin-friction lines as presented by Martinuzzi and Tropea[18] and time-averaged friction lines on the floor calculated from IDDES simulations are shown in figure 5.6. The patterns are strikingly similar. The two small recirculation zones along the sides of the cube as well as the two large primary recirculation regions near the base of the cube are well predicted. The two recirculation zones behind the cube mark the base of the arch-shaped vortex manifesting energy from the shear layers separated from the top and sides of the cube[17].
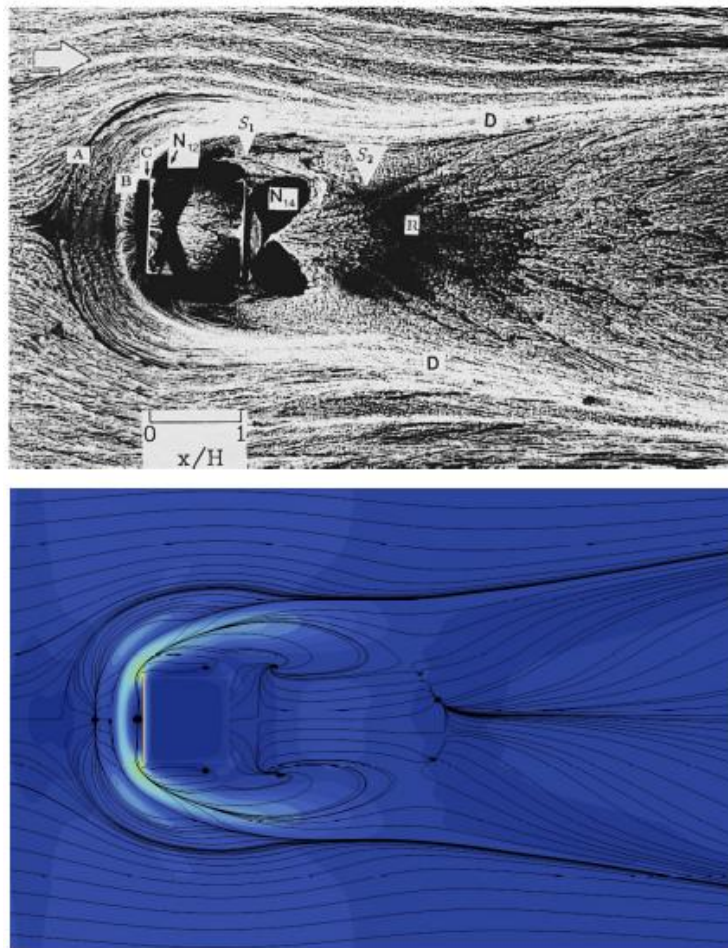
Figure 5.6: Time-averaged surface-constrained streamlines on the ground and experimental skin-friction lines on the floor[18]

Finally, figure 5.7 shows the flow features as predicted by the modified IDDES

simulation generated using the isosurfaces of the second invariant of velocity gradient(Q*=50). The flow predictions are in very good agreement with the experimental findings. The horse-shoe vortices and its extension into the far wake and the arch-type vortex behind the cube base can be clearly seen.
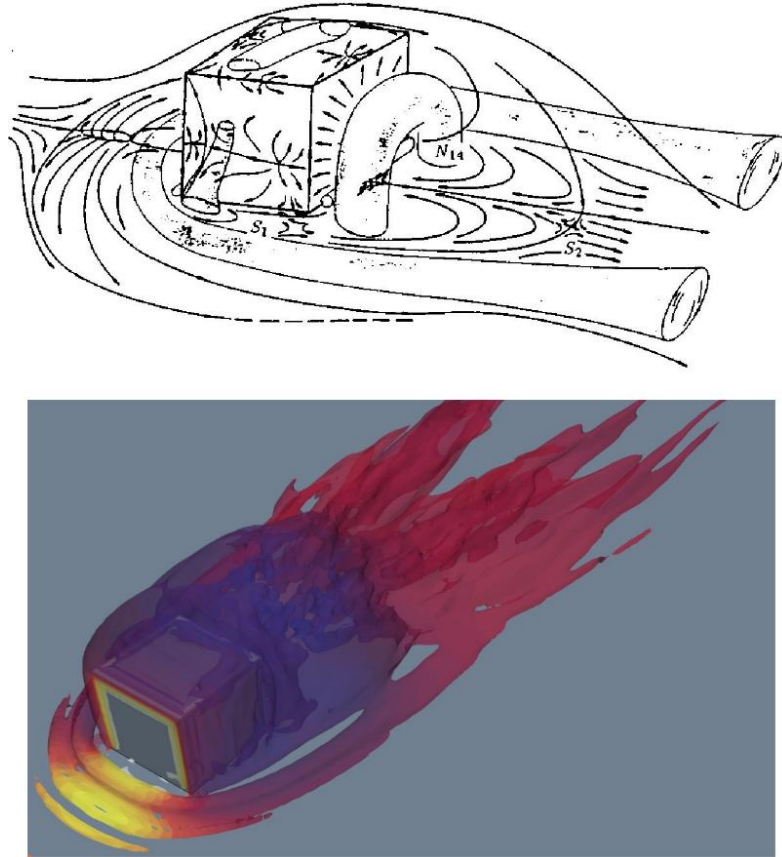
Figure 5.7: Isosurfaces of Q-criterion(Q^*=50) showing the horse-shoe votrex system, the arch-vortex and other flow features as predicted by the modified IDDES simulation in comparison with a schematic representation of flow around a surface-mounted cube[16]

From the above findings, it is clear that the IDDES-SST model with modified coefficients has an overall superior performance to that of the other models although the flow predictions are fairly good at some other areas. The final force coefficient values and the recirculation region length as predicted by URANS and IDDES simulations are presented in table 5.1. The coefficient modification has also helped improve the heavy under prediction of the lift coefficient by the default URANS model.

Table 5.1: Force coefficients and recirculation region length behind the cube as predicted by URANS and IDDES for Re=22500

	URANS(default)	URANS(modified)	IDDES(default)	IDDES(modified)
C_D	1.077	1.091	1.2	1.254
C_L	0.321	0.579	0.427	0.522
X_{RB}	5.3	2.8	3.5	2.5

Since there is an ambiguity in the force coefficient values in this particular Reynolds number. We carried out the same simulation at a Reynolds number of 5610 and compared the results with Curley's findings in his DNS study[17]. The results are within acceptable agreement with the DNS calculations. The values are compared in table.

Table 5.2: Force coefficients as predicted by current setup at Re=5610 compared to Curley's DNS calculations[17]

	DNS	Current CFD	% variation
C_D	1.317	1.221	+7.29
C_L	0.533	0.563	-5.63

5.1   Results and Discussion

Once, the CFD model was validated, the second cube was brought into the setup as an overset region. A block was placed around the rear cube to create the overset region. This block extended to equal the dimensions of the inner most volume source around the lead block and had grid settings alike as can be seen in figure 5.8. The second volume source outside this inner volume source for the lead block acted as the overlap region. The ground of the overset was placed to coincide with the ground of the tunnel. This block along with the rear cube can be moved as a whole region and hence carries the local mesh refinement with it. The ground plane was given a no-slip condition along with the surfaces of the cube. The overset region was then

interfaced and connected with the background region containing the lead cube. This ability of overset to be manipulated as an independent region and then being able to be connected to the background domain in the biggest benefit in choosing the overset meshing methodology besides the savings in mesh size.
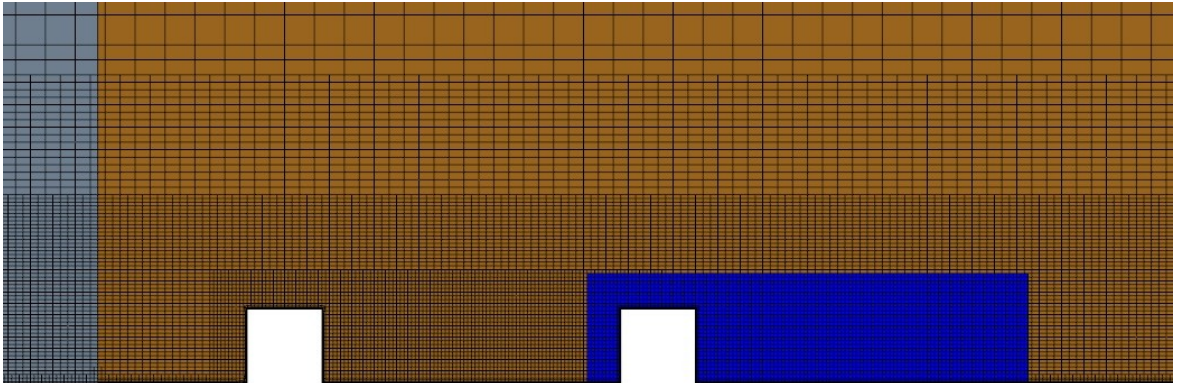
Figure 5.8: Mesh along Y=0L plane for the case with tandem cubes

Now, we will detail the ability of this method to replicate the work of Martinuzzi and Havel[25] with tandem cubes at different inter-cube spacings. This whole study was to validate our simulation methodology so that we can apply the same to the DrivAer setup and investigate the interferences during platooning of ground vehicles. Figure 5.8 shows the overset region in the background domain and the mesh used along the vertical symmetry plane.

5.1.1   Body Forces

Drag coefficient trends, based on frontal area and free-stream velocity, at different inter-cube spacings was presented by Martinuzzi and Havel[24]. Martinuzzi et al. identified three distinct flow regimes based on obstacle spacing. When S/H<1.5, where S is the inter-cube spacing and H in the cube height, vortex shedding is interrupted and periods of random fluctuations were picked up by the frequency spectra. In the lock-in regime, 1.5<S/H<2.5, vortex shedding is continuous and the frequency of shedding scales linearly with the S. A bistable regime(4<S/H<6), where two non-harmonic shedding frequencies appeared ,was recorded. For larger spacing, the shed-

ding frequency asymptotically approaches the isolated values. The trends of the drag coefficient is dependent on this frequency of vortex shedding. The C_D transitions smoothly from the intermittent to the continuous shedding regimes. For the lead cube, C_D initially decreases, reaching a minimum at the end of the lock-in regime. We picked four different positions in these regimes to validate the data. The trends obtained from the current CFD study matches considerably well with the work of Martinuzzi and Havel[24] and is shown in figure.
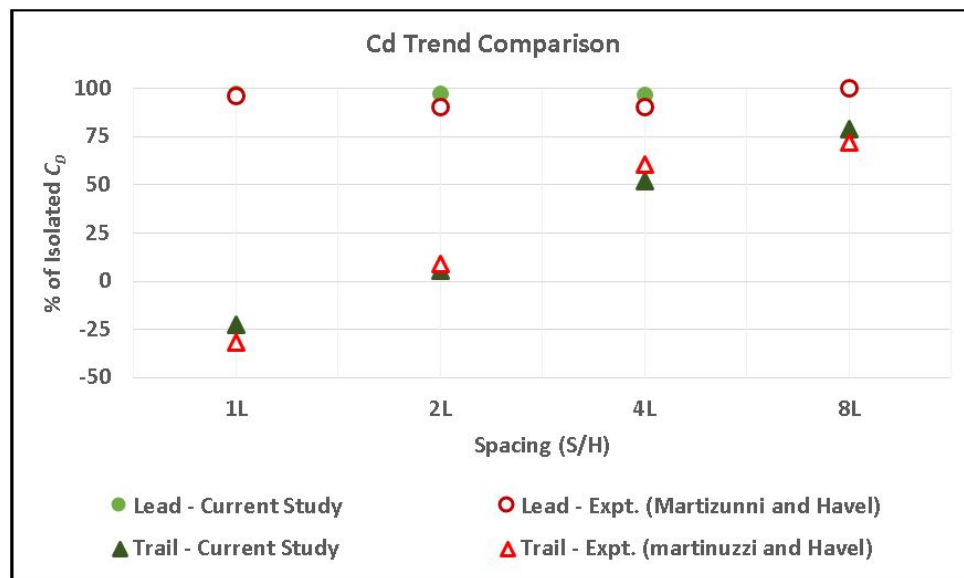
Figure 5.9: Drag coefficient vs S/H comparison between experimental results and current CFD

There are minor discrepancies in the level of drag predicted by our current CFD work. This is again due to the fact that the experiment was done in a channel setup and the current work has almost zero interference from blockage effects. Hence, we move forward to compare the flow features predicted by our current CFD to ensure its predictions capabilities are good enough to move forward with the DrivAer study.

5.1.2 Mean Flow and Wake Structure

To validate the CFD setup on the prediction of flow interaction between multiple bodies, we investigate the mean and instantaneous flow fields around the cube and

compare the results with experimental data[25, 24]. To investigate this we chose three different inter-cube spacings each to represent a different frequency regime(S/H=4,2 and 1). The main flow features visualized and detailed by Martinuzzi et al. would be used to compare and contrast the differences, if any, between CFD and the experimental results. A few intricate details at S/H=2 will also be discussed as this is representative of the lock-in regime and some intersting flow interactions happen during this spacing.
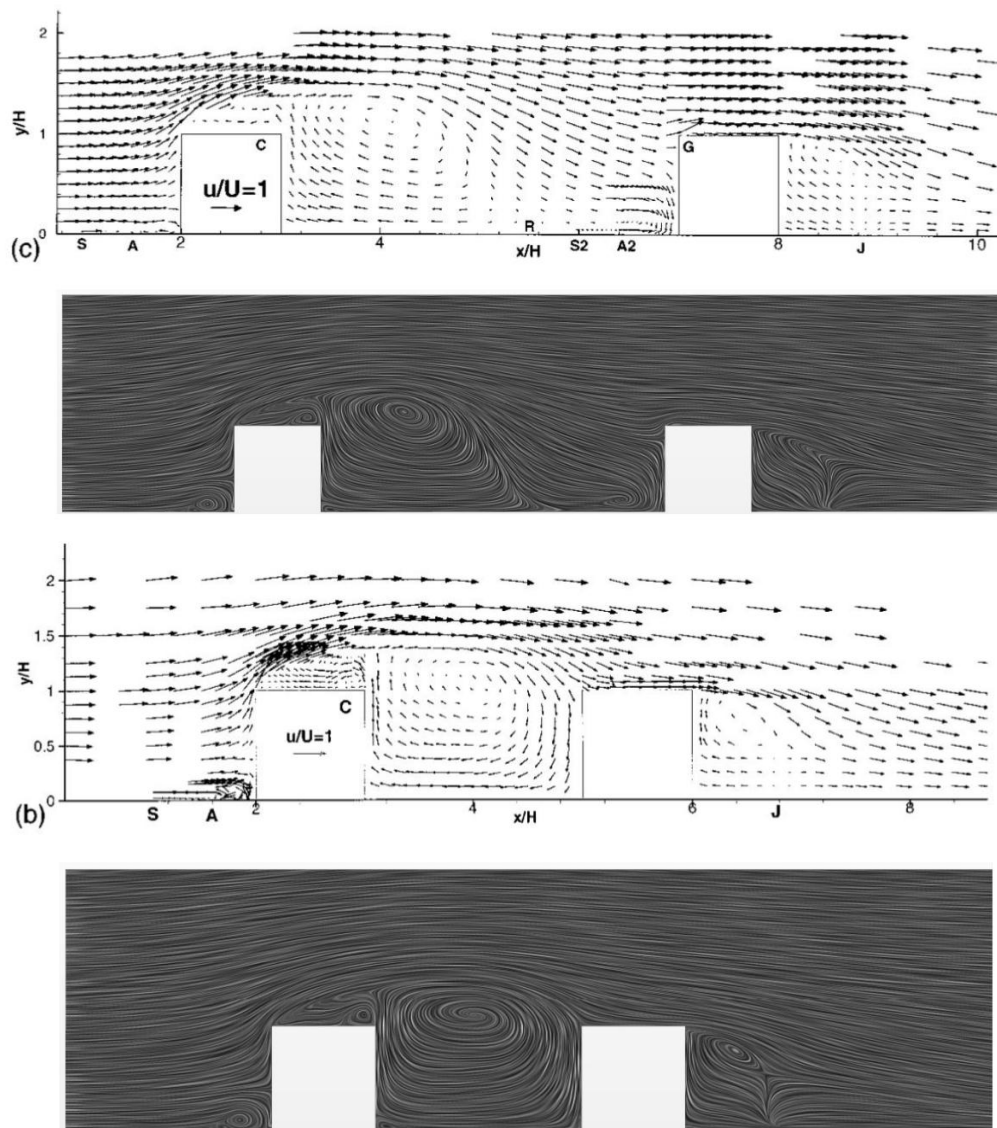
Figure 5.10: Mean velocity vector fields along Y/H=0 at:top-S/H=4 and bottom:S/H=2

If the current setup captures these flow changes, the CFD setup can be deemed good to go ahead with DrivAer studies.

Time-averaged velocity vector fields are initially analyzed along the stream wise plane of symmetry and are shown in figure 5.10. The CFD calculations at both the spacings reveal a primary recirculation region behind the cubes. The rear cube has this to be a smaller region because of the turbulence generated in the wake of the lead cube and the flow not being able to regain free stream conditions at even S/H=4. At S/H=2, the vortex core behind the lead cube is marginally larger and slightly distorted than calculated in experiments and yet the overall shape of the wake and the two main recirculating regions appear to have been reproduced with good accuracy.

The grid independence studied for URANS was directly utilized for IDDES owing to time restraints and also considering the fact that it is almost the size of the Taylor micro-scales computed. This might be a reason for the wake distortion. The mean flow measured at a horizontal plane for the cube spacings are shown in figure 5.11.

For lack of measurements for S/H=4, only the CFD calculated vectors are shown. The figure shows two counter-rotating recirculation vortices in the inter-cube gap and downstream of the rear cube in the wake. The vector scenes also suggest the influence of the the flow impinging on the leeward face of the rear cube on the shear layers emanating from the side faces of the rear cube. This is supported by the flow predictions of Martinuzzi et al. This is the reason for large scale oscillations of the wake flow to lock-in with the gap flow[25].
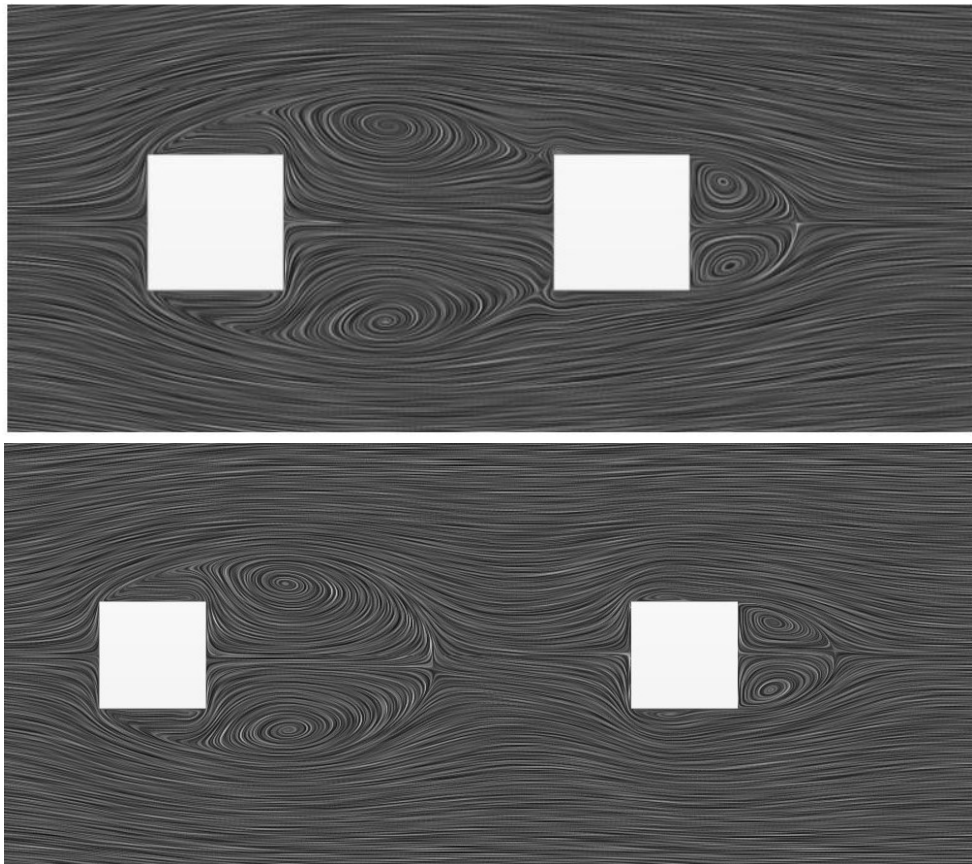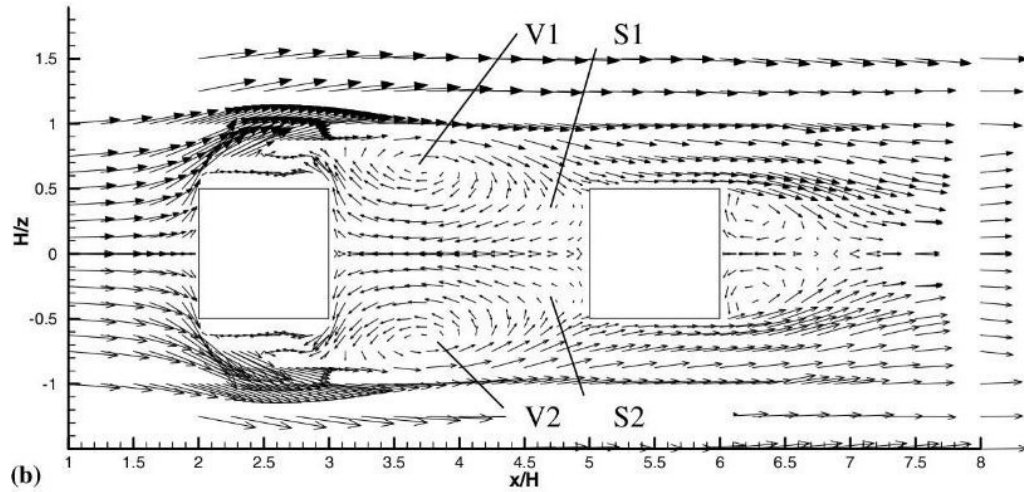
Figure 5.11: Mean velocity vector fields along Z/H=0.375 at:top-S/H=2 and bottom:S/H=4

The pressure recovery is also captured very well as can be seen from the right end of the images and as shown in figure 5.12 for S/H=2. Spurious vortices are seen to emerge from the upper and lower leading edges of the rear cube which might be due

to the mis-interpretation of grid refinement as wall proximity as discussed by Paik et al.[37]. This will cause premature switch to unresolved DNS where the local cell Re is small making it a source of error. The recirculation region downstream the rear cube seems unaffected by the cube spacing, which is consistent with the experimental measurements[25].
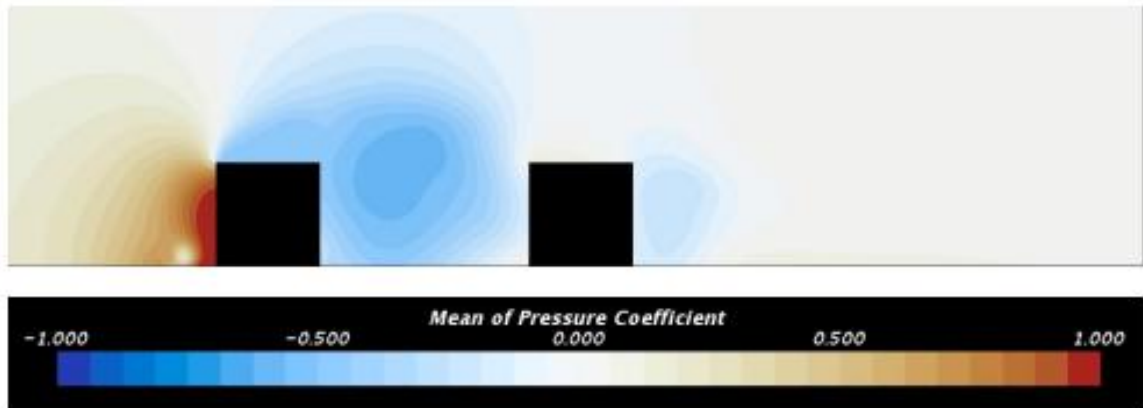
Figure 5.12: C_P distribution in the inter-cube spacing at S/H=2

Figure 5.13 shows the location of horse-shoe vortex(HSV) at 1H behind the lead cube at a cube spacing of 2H. The CFD calculations are spot on with respect to the experimental results. The location of HSV is independent of the Reynolds number but only influence by the upstream conditions(inlet). The location prediction is spot on because of the correlation between CFD and experimental boundary layer thickness. The complex structure of the horse-shoe vortex, dominated by multiple vortices, as revealed by the smoke visualizations of Martinuzzi is well predicted by out current work although the location of the primary stronger vortex is closer to the cube windward face than seen in the experiment as seen in figure 5.14.
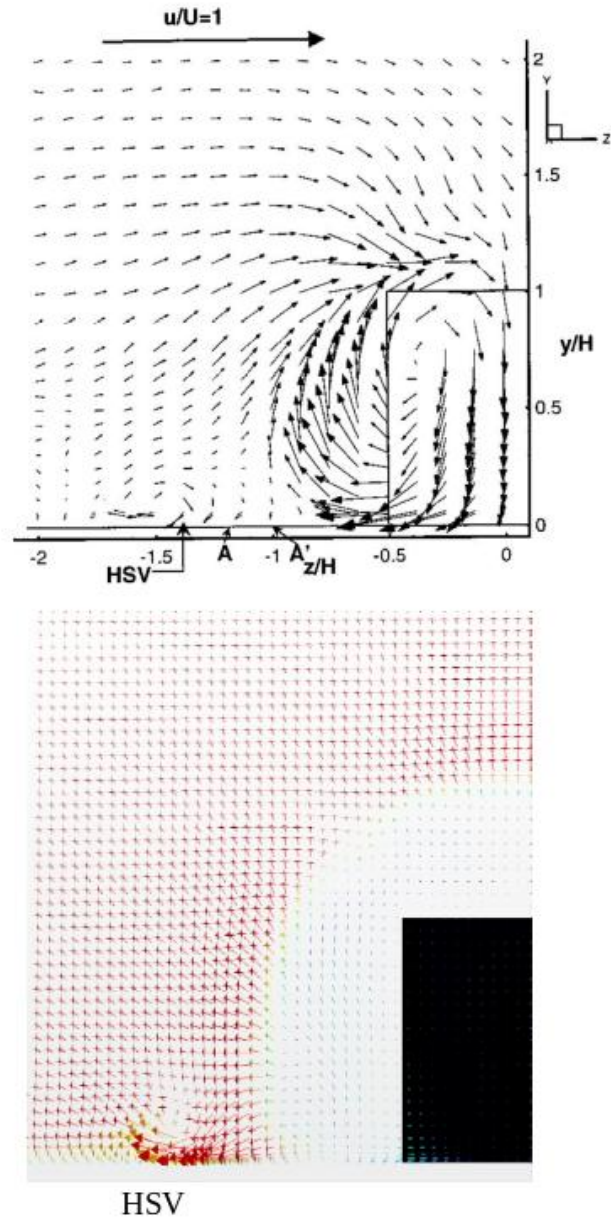
Figure 5.13: Location of HSV at S/H=2:Experiment(top)[25] and CFD(bottom)
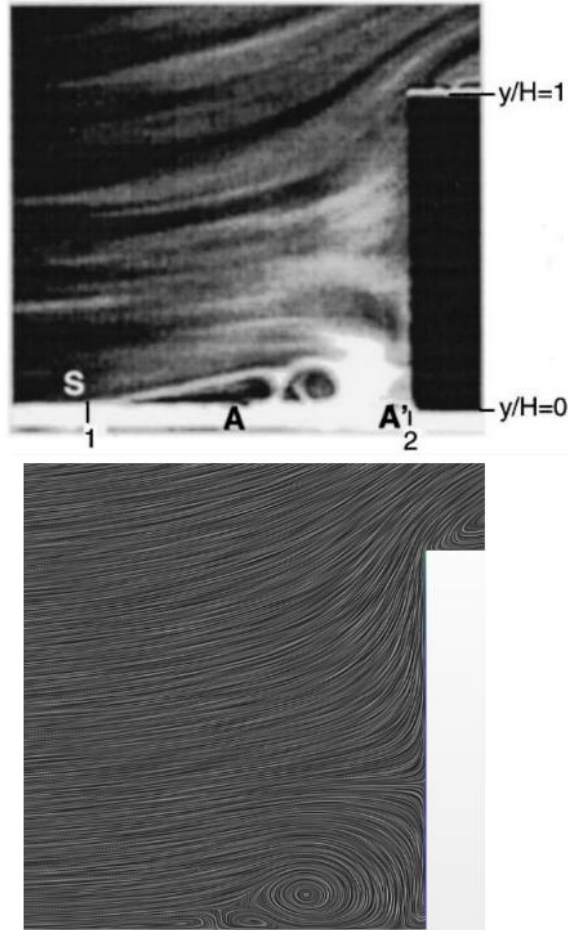
Figure 5.14: Complex structure of the Horse-shoe vortex at the stagnation of the lead cube at S/H=2:Experiment(top)[25] and CFD(bottom)

Figure 5.15 shows the flow over the top surface of the upstream cube where the shear layer separates at the leading edge and forms a recirculation zone. The interplay among the shear layer and backflow from the inter-cube spacing with it separating at the trailing edge plays a vital role in this. This recirculation zone is characterized by multiple recirculating vortices above the cube top surface. IDDES slightly over predicts this recirculation which is in conjunction with the findings of Paik et al.[37]. Thus, reversed flow along the top surface of the cube is underestimated.
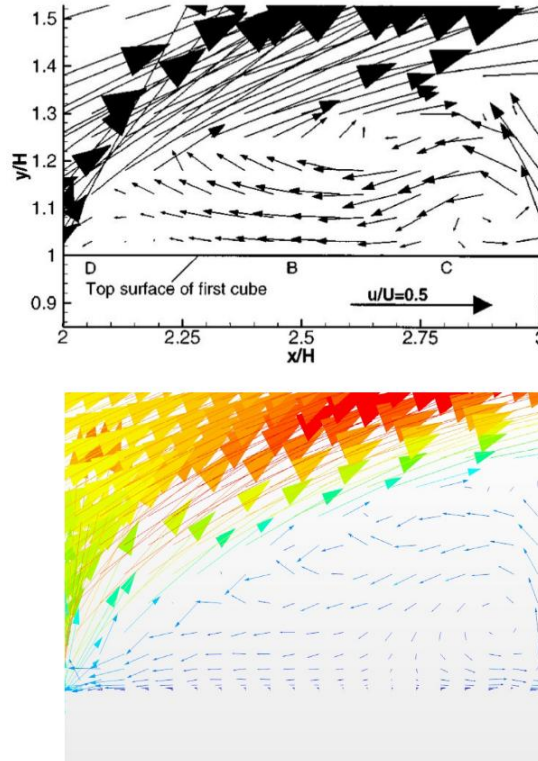
Figure 5.15: Mean velocity vectors at Y=0 plane over the top face of the upstream cube:Experiment(top)[25] and CFD(bottom)

Finally, a comparison between the oil-film flow visualizations on the floor as reported by Martinuzzi and Havel[25] and the surface constrained friction lines colored with wall shear stress magnitude are drawn. This gives an overview of how well the simulations could predict surface shear stress patterns which is very important for studying flow over cars. The results are shown in figure 5.16. Two distinct lines wrapping around the upstream cube marks the horse-shoe vortex inducing high shear region on the plate.The upstream line S(shown in experimental image) marks the line along which the boundary layer undergoes three-dimensional separation due to the adverse pressure gradient. Footprints of a pair of counter rotating vortices are seen just downstream of the lead cube for both spacings. All these features seem to be insensitive to the spacing between the cubes. An inward deflection of the shear layers S and A in between the cubes, around midway, is also noticeable after which it is deflected away. This lateral deflection is much stronger for S/H=4 than for S/H=2.

All these features are well captured by the current IDDES simulations as seen from figure.
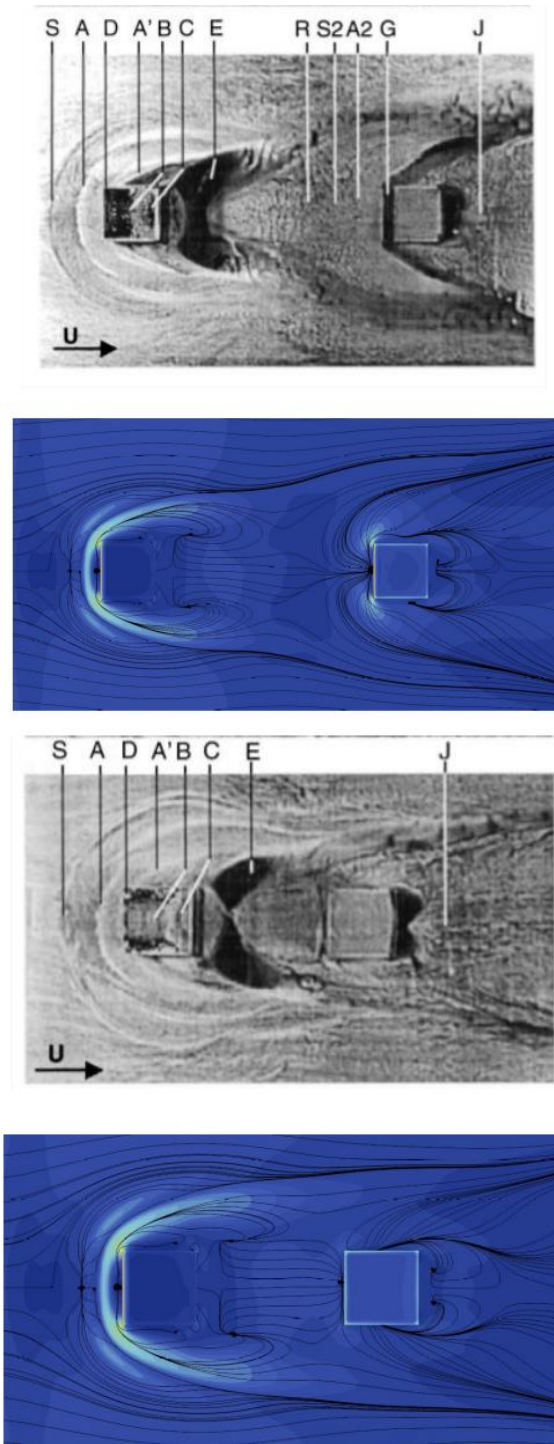
Figure 5.16: Time-averaged friction lines compared against experimental oil-flow visualization[25]:topS/H=4 and bottom-S/H=2

Normalized turbulent kinetic energy is used to represent the turbulence field in all 3 cube spacing situations. The change in turbulence levels in the upstream region of the first cube with respect to cube spacings is negligible. The impinging of the shear layers on the windward face of the rear cube creates a spike in tubulence levels around that region. The turbulence levels are much lower in the inter-cube spacing at S/H=1 than for S/H=4. This is in parallel with the reports of Martinuzzi et al.[25]. The primary recirculation region in the wake of the rear cube exhibits elevated levels of turbulence with increase in inter cube spacing. The leading edge top-face separation on the second cube enclosing the small separation bubble is also captured very well which is marked by high turbulence levels as seen in the figure for S/H=4.
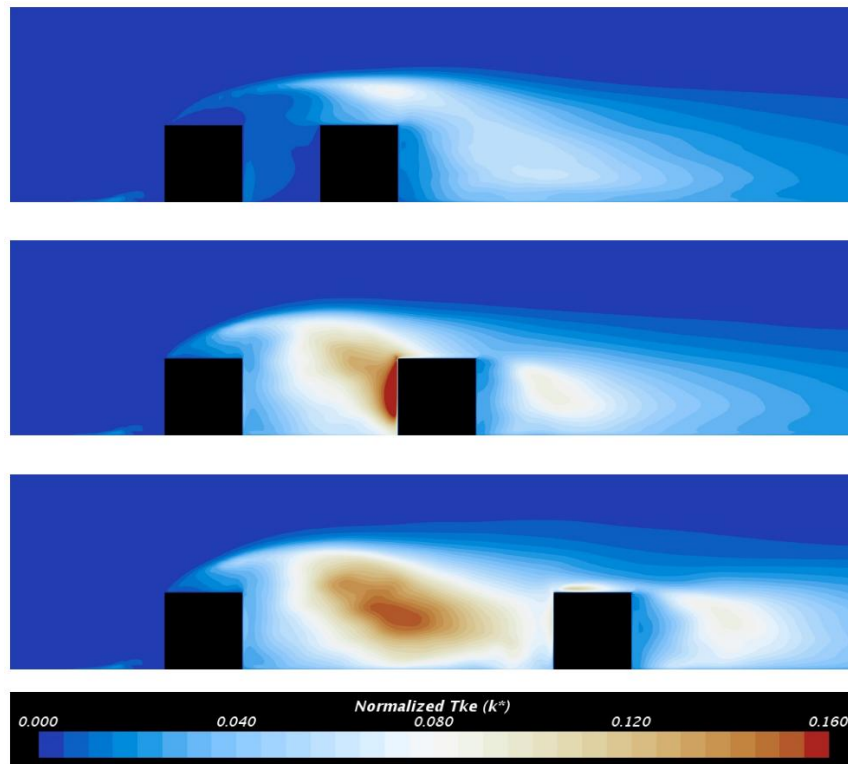
Figure 5.17: Scalar scenes of Normalized Turbulent Kinetic energy along Y=0 plane for S/H=4(top), 2(middle) and 1(bottom) as computed from current study

5.2   Concluding Remarks

This study was aimed to develop a simulation technique for obtaining body forces and flow fields for a bluff body when it is brought in the vicinity of another with the pay-off being able to use this towards on-road ground vehicle platooning and drafting situations. The mesh and turbulence modeling was validated with experimental results before bringing in the second bluff body. A modification to the current available SST-IDDES turbulence model was proposed and is proven to perform better for this particular case simulating boundary layers, large separating shear layers and high energy, high vorticity turbulent wakes. Although this needs further investigation, that is not the ultimate goal of this thesis work. With regards to bluff body interaction, as proposed by multiple work earlier, there is a significant influence by the vortex and shear layer interaction on the drag induced on a body. The drag of the rear cube went to a negative value at closer spacings creating a suction effect on the cube. The flow features in the inter-obstacle spacing seems highly affected with change in the obstacle spacing. The wake downstream of the rear cube seem unaffected by the spacing which was expected. The turbulence levels in between the cubes seems to vary much depending on the cube spacing which would play a vital role in the study with the fastback DrivAer models.

CHAPTER 6: DRIVAER DRAFTING

In this study, we focus on the aerodynamic interference effects caused during a platoon or a drafting situation of a modern road vehicle model, the DrivAer fastback variant developed by Heft et al.[1] by applying the knowledge gathered from the cube simulations. As discussed earlier a considerable amount of work has been done on understanding the concerned on-road situation and the aerodynamic impact of such a scenario on individual vehicles. But, to the author's knowledge, all of the work has been done on simplified bluff bodies, such as the Ahmed body. The DrivAer model was created to provide a more realistic car geometry that is generic and open to research and thus transfer of data. This was done mainly to close the gap, if any, between the Ahmed body, the SAE bodies and a realistic car of today. While the above mentioned reference geometries have been a great source of knowledge to discern the flow features around a ground vehicle, there are significant simplifications made to make it easier on the computational requirement front. Hence, DrivAer model is the current model of choice and has become the focus of research lately. The fastback variant of the DrivAer geometry was selected for this study owing to the data available on vehicle platooning with 25deg Ahmed bodies which are comparable to the fastback type ground vehicle. In addition, a detailed version of the variant was chosen with closed grilles to see the impact of the detailed underbody, the mirrors and the pumping effect of the wheels on the wake of the model to contrast the differences on flow between the current model and the Ahmed body. Overall dimensions and geometric details can be seen in figure 4.7 illustrated in chapter 4, noting that a 40% scaled model was used. Scaled models are used to reduce overall computational costs. Restraints are used during wind tunnel testing as shown in figure 6.1 and the force

data computed has to be corrected as these restraints serve as a potential source of error. The setup will be validated first for an isolated DrivAer simulation and then a rear trailing model will be brought in, to study the interference effects on force coefficients and flow fields.
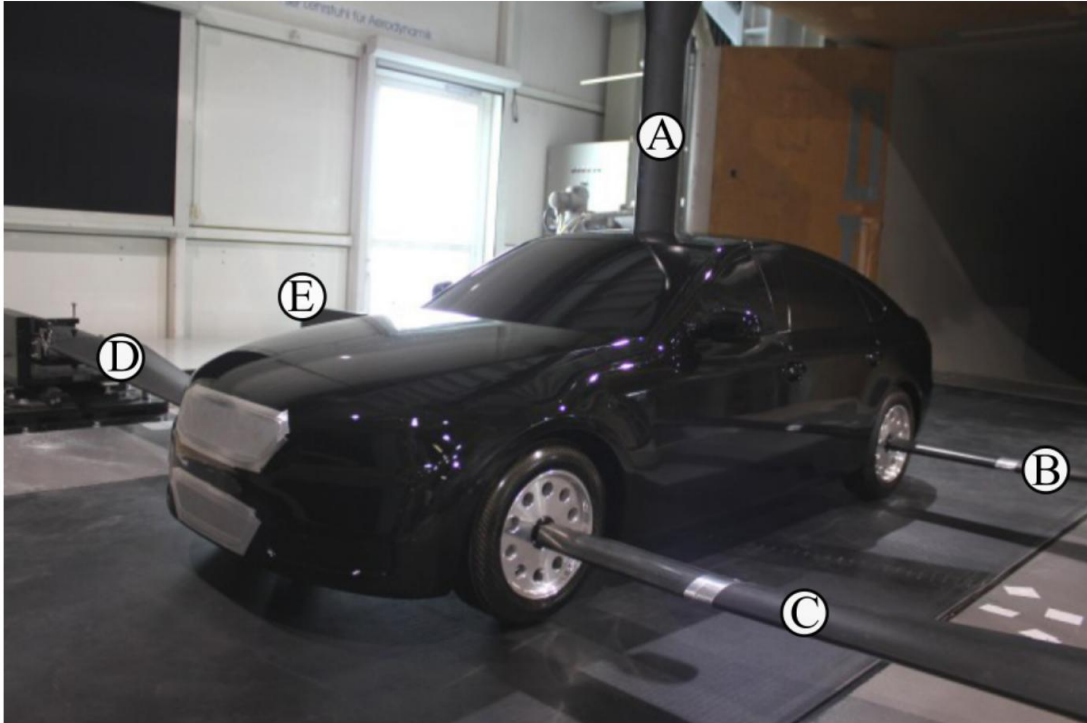
Figure 6.1: The tunnel setup as used by Heft et al.[1] showing the restraints

6.1 Model Validation

In this section, we compare the results from the current study against experimental data available for validation. The IDDES-SST model with modified coefficients was the only model used in this study as it was superior to all other models for this particular scenario as discerned from the cube studies. The validation was done with the same setup as in the drafting setup except for the rear car model removed from the domain. A constant time step and Reynolds number have been maintained through both the isolated and drafting cases. Several areas has to be addressed while evaluating and comparing CFD data to experimental data. The method of constraint used in the tunnel to hold the vehicle in place and the the measurements/data acquisition

techniques. As seen from figure 6.1, there are five restraints attached to the vehicle which would obstruct the flow field. They affect the flow field in spite of being streamlined and hence, their influence on data collected should be noted. On the contrary, CFD is done without any restraints in place as the force data are reported through the integration of surface pressure and skin friction. Additionally, there is an issue with repeatability in experimental results as a change in position of the test body or the type of nozzle used can heavily affect the results[38]. Thus, the current CFD data has been corrected to draw a closer comparison with experimental data.

Table 6.1: Overall force coefficients as predicted by current CFD after correcting for the restraints.

	CFD	Expt. (Heft)
C_D	0.268	0.275
C_L	0.089	-
L/D	0.332	-
C_{LF}	-0.036	-
C_{LR}	0.125	-

The Overall force coefficients computed by our setup, after the correction for restraints as suggested by Collin et al.[38], is presented in table 6.1. Total C_D value was under predicted within 3% which is well within acceptable accuracy. Figure 6.2 compares the C_P data computed over the vehicle top surface along the vertical plane of symmetry where the current CFD results are in good agreement with experimental data. However, for X=0.5m, the leading edge of the roof, and at X=1.2m, at the rear end of the roof, there are some discrepancies. The under prediction at these areas are most likely due to the absence of a stinger as in experiment shown in figure 6.1 or a difference in the manufactured DrivAer's windshield to roof transition.
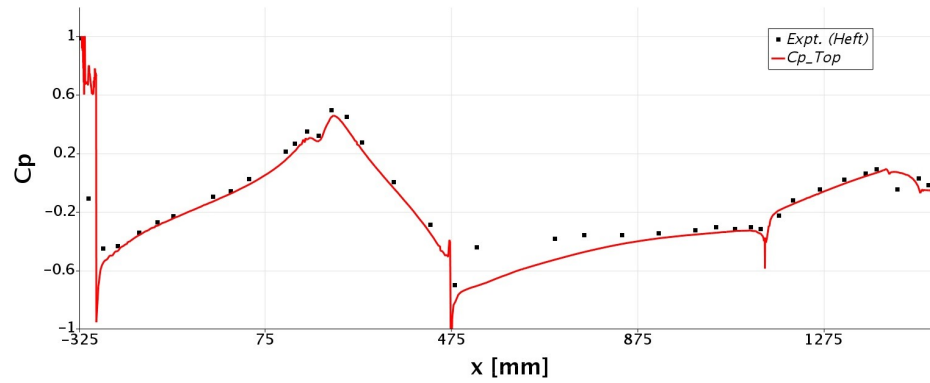
Figure 6.2: Pressure coefficient over the top of the vehicle at centerline Y=0 of current IDDES simulation versus experimental data[1]

Figures 6.3, 6.4 and 6.5 shows the entire surface C_P distribution over the vehicle with detailed comparison at specific areas from the experiment. As discussed earlier, a recirculation zone can be noted at the cowl based on the marked high pressure region. The lowest pressure coefficient occurs at the A-pillar, side mirrors and the front tire.
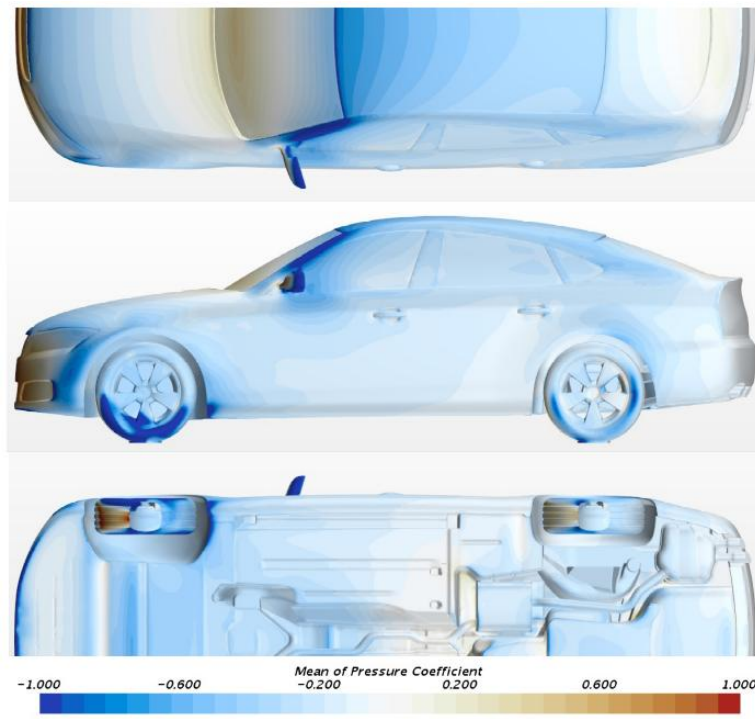
Figure 6.3: Pressure coefficient distribution on top,side and bottom surfaces of the DrivAer
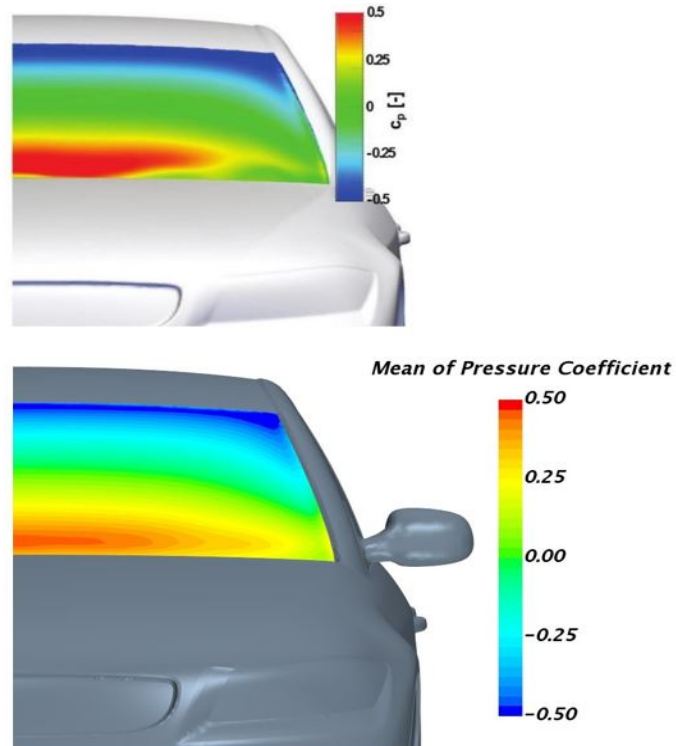
Figure 6.4: Pressure coefficient distribution over the front windshield
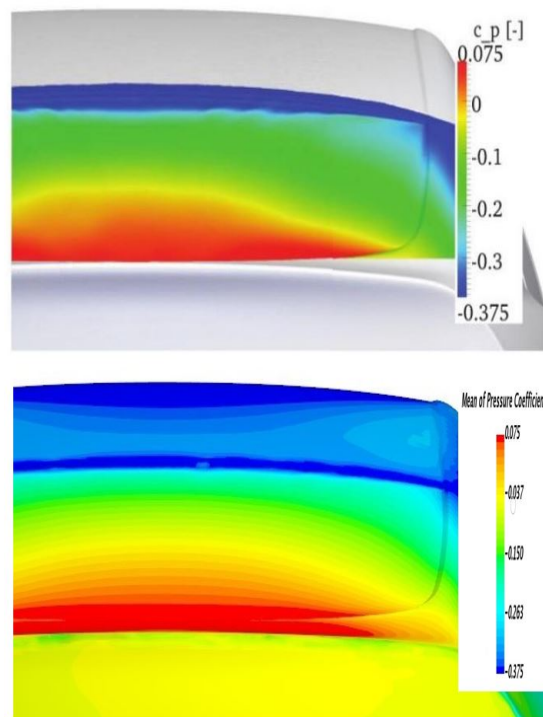
Figure 6.5: Pressure coefficient distribution over the rear windshield

To understand the wake flow field, vector scenes using line integral convolutions of mean velocity were computed in the symmetry plane of the flow field. Figure 6.6 shows two counter-rotating vortices and a saddle point, marked in red, at a distance of 0.17L from the rear end of the car. The work presented by Strangfeld et al.[39] supports our current results as the predictions are in good agreement. A separation in the rear glass with a reattachment near the trunklid was also noticed.
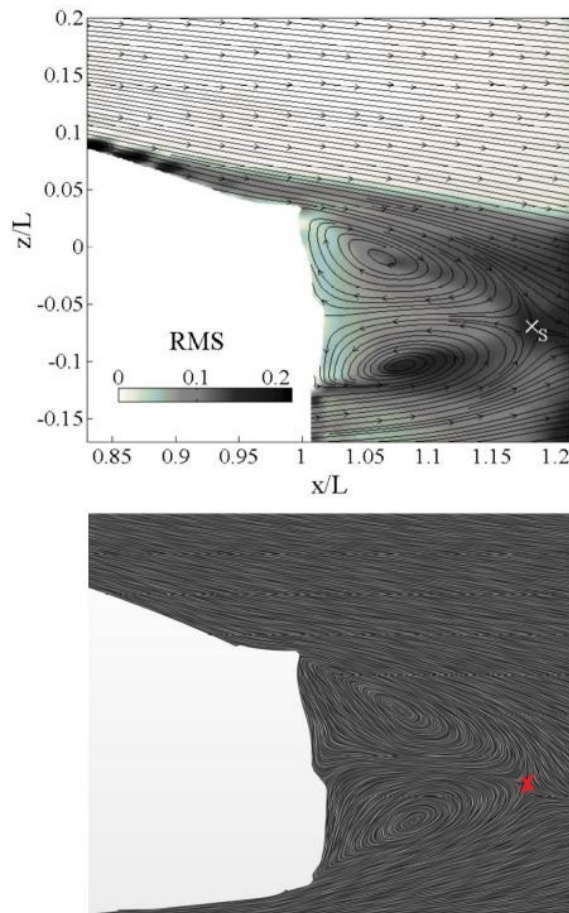
Figure 6.6: Vector scene showing the computed wake of the DrivAer vehicle compared with the streamlines of velocity as presented by Strangfeld et al.[39]

Additional information regarding the vortices generated off the pillars are shown in figure 6.7. The isosurfaces show a concise vortex formed at the edge of the roof near the base of the A-pillar and progresses rearwards over the roof towards the rear of the vehicle. This was as detailed by Heft et al.[1] as they describe this A-pillar vortex to

form a cylindrical vortex structure at the junction of the roof and the rear windshield. CFD work on DrivAer models that has been presented so far fail to reproduce this feature as they predict the A-pillar vortices to extend beyond the roof into the wake. Additional features such as the C-pillar vortices, wake off the side mirrors and the front wheels were also made visible.
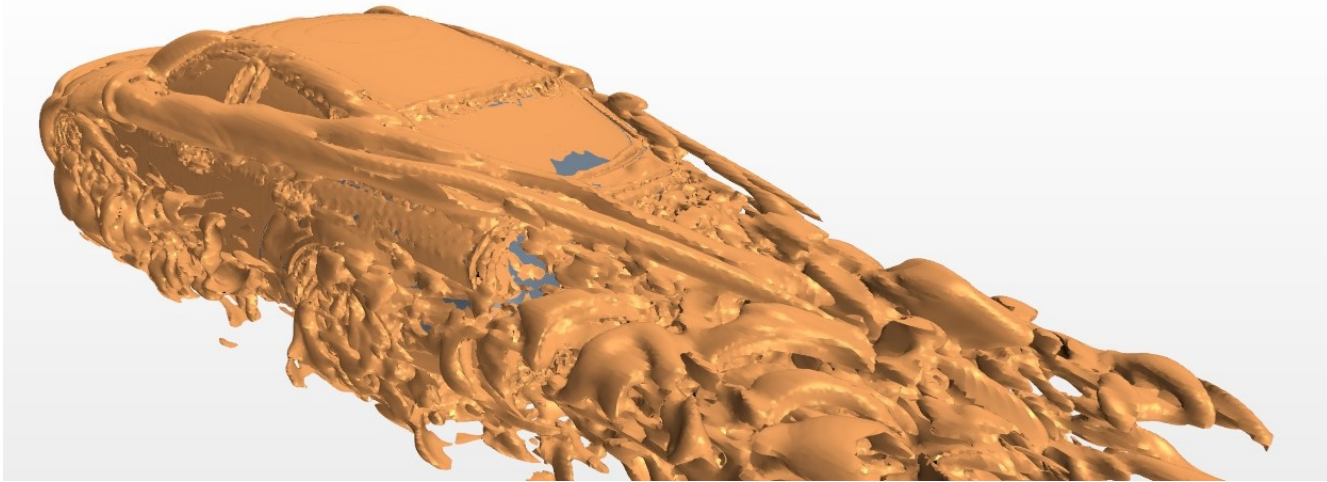
Figure 6.7: Isosurface of Q-criterion(Q^*=50)(averaged flow)

Now, we focus on the ability of the current setup to resolve the far wake of the car. The wake predicted by IDDES behind the fastback model extend almost up to 4 car lengths as seen in figure 6.8. The wake of the DrivAer model was expected to be larger than the Ahmed model's wake because of the geometric details, the wheels, the mirrors, all of which contributes in the generation of vorticity that extends the wake. Although no experimental data is available to compare or contrast our wake data with. Since our grid technique and simulation methodology predicted the flow features of the complex wake behind the cube accurately, we believe our results should not be far away from the actual values. The only possible source of error would be a premature switch between RANS and LES in the wake because of the high Reynolds number. The IDDES filter depends highly on the grid size to resolve or model the eddies in the particular region. This switch is influenced highly by the grid size

used in the domain. The mesh and grid refinement used in this study is based on the information derived from the study conducted on surface-mounted cubes. The increase in Reynolds number was also considered while deciding the grid size and its distribution. This grid methodology is also very similar to what is being used in most of the literature on simulating on-road vehicles. So, the probability of the grid size being the source of error is very small. Although a study on the influence of grid size in the far wake resolution of a detailed fastback DrivAer model is desired in the future.
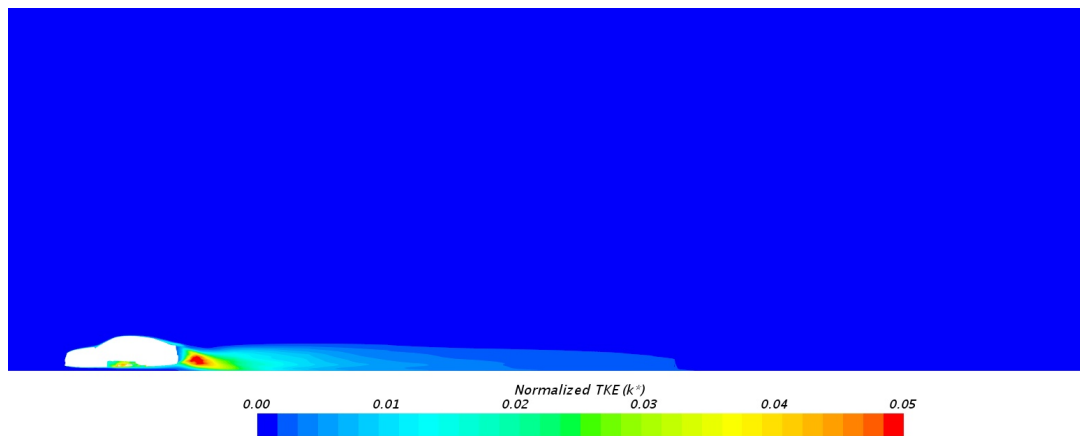
Figure 6.8: Normalized TKE(top) and Normalized Velocity(bottom) on the symmetry plane Y=0L showing the wake predicted by IDDES simulation

The figure shows scalar scenes of normalized total turbulent kinetic energy along the symmetry plane Y=0L. This contradicts most of the predictions in literature on the Ahmed body with a 25° backlight angle, where a wake length of much lesser magnitude has been reported. Several studies on Ahmed body platoon from the past have documented that the rear model returns to an isolated state almost at around 2-4 car lengths and some of these studies were conducted using URANS simulation with a fairly similar grid[31]. Experimental data shows Ahmed bodies to return to isolated state 2 car lengths behind the lead model. This shows that ideally Ahmed

body wakes are less than 2L behind the base. The difference in wake length would be an important factor in the drag changes during a platoon of DrivAer models.

With the current setup, a total of about 28 million cells for the isolated DrivAer geometry, the simulation required over 150 hours on 96 x 2.4 GHz Intel Xeon E5-2665 processors to run through 36 LETOTS. When we consider the platoon case, which had a total cell count of about 58 million cells, it takes at least more than twice the computational requirements as the single DrivAer case. Now, if we try to resolve the mesh more to get a better resolution to resolve the far wake, the mesh size would reach over 80 million cells for a single DrivAer case and over 150 million for the platoon case. The author tried resolving the wake mesh better by extending the volume sources behind the car farther which ended up with a cell size of about 52 million cells. But the wake was still as long and the deviation in the force predictions were negligible. Hence, we can expect broad trends on how DrivAer geometries, which represent an actual car, interact with each other in a convoy or platooning scenario with the 27 million cells case. Therefore, the author decided to go forward with the study in hopes of gathering some base data as a study on multiple DrivAer geometries has never been done to the author's knowledge at the current time.

6.2 Results and Discussion

In this section, we focus on the effects of aerodynamic interferences on road vehicles in platoon using the DrivAer fastback variant. The simulations were run for 10800 time-steps and are averaged over 8000 time-steps to get the mean flow field and force data. The trailing car was brought in similar to the cube setup as an Overset region and was meshed independently. The mesh refinement is similar to the lead car with the refinement sources following the body shape of the car and wake refinements done using rectangular volumes up to a length of 4L in constant progression. Figure 6.9 shows the mesh with the trail car brought in.
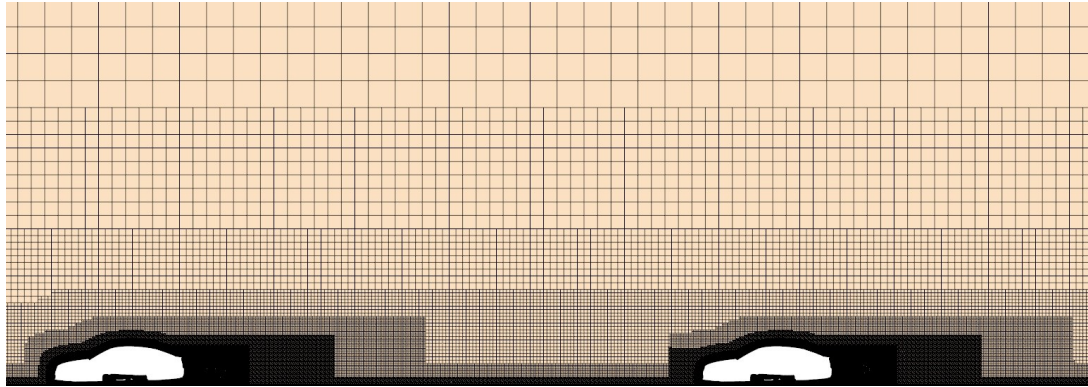
(a) Y=0L Plane
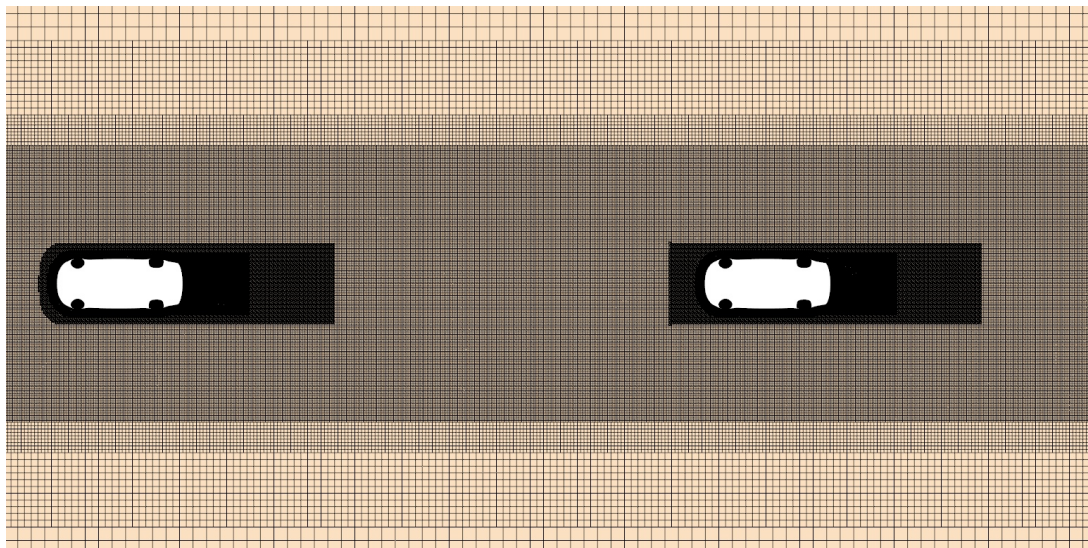
(b) Z=0L Plane

Figure 6.9: Mesh slices of domain for the DrivAer platoon

The overset was moved for every longitudinal spacing and then re-interfaced and the solution was computed fresh from the start for the new spacing. Figure 6.10 shows the variation of drag for the lead and trail DrivAer geometry at different longitudinal spacings. Force data presented shows that the trailing model is affected by the lead model wake even at 4L distance behind the leading model base. This is due to the longer wakes of the DrivAer model and hence the trail model does not return to an isolated state even at this large spacing. Drag trends are similar to predictions from Ahmed body studies done earlier by Pagliarella[4] and Rajamani[31] but the

magnitude of the drag change is less pronounced. The leading model drag decreases throughout the spacing and the trailing model drag increases through the same range of spacings. The net drag of the platoon is always reduced.

Pagliarella associates this drag penalties to vortex interactions between the two models. Watkins'[6] and Pagliarella's[4] results suggested that the C-pillar vortices that are generated off the rear of the leading model creates a downwash in the near wake behind the base. The vortices thus impinges on the nose of the trailing model, creating a region of high pressure at the frontal surface. This impingement causes movement of the trailing model stagnation point normally up on the surface as well when the longitudinal spacing is reduced.
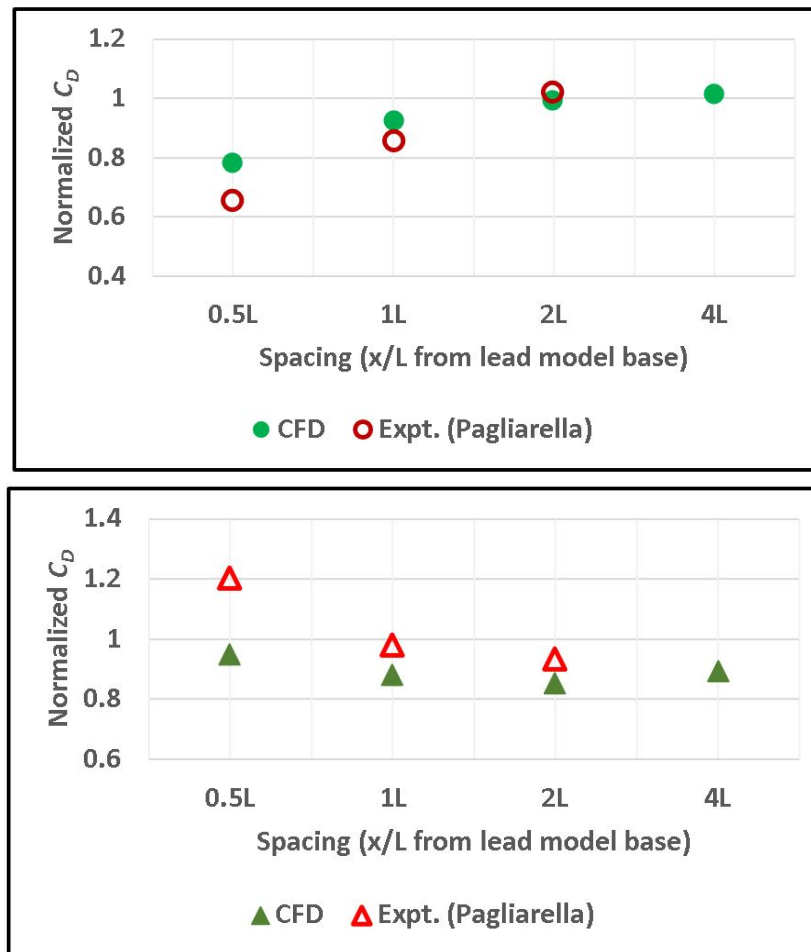
Figure 6.10: Drag coefficient for lead and trail models in platoon at difference longitudinal spacings

Figure 6.11 supports Pagliarella's predictions. The presence of the trailing car in close proximity to the leading car curtails the space for the vortices off the lead car's rear to develop. Bull et al., stated that the feedback along the relevant leading model separating shear layers affects the formation of vortices. This creates a high pressure region in the space between the two vehicles due to the velocity deficit in the gap. It is also seen from the $\omega_Y{}^*$ scalars as shown in figure 6.13 that IDDES predicts eddies from the lead model to travel as long back as 4L and are not diminished and hence the reason for the trailing model to fail to get back to the isolated state.
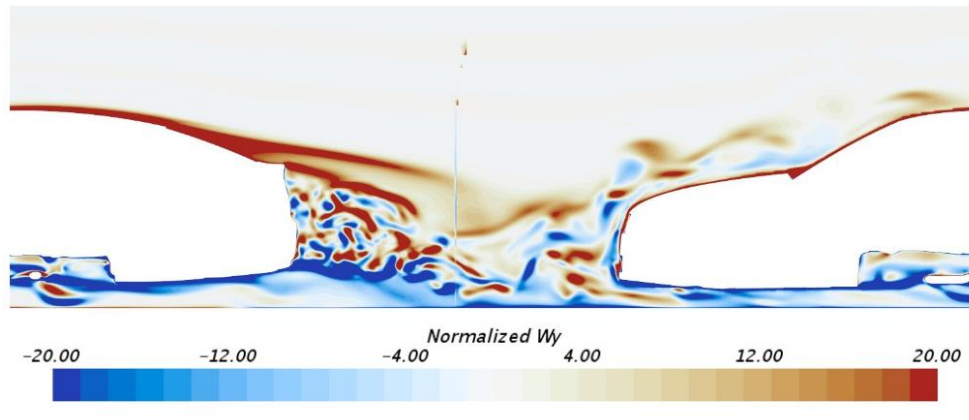
Figure 6.11: $\omega_Y{}^*$ along Y=0L plane showing vortex impingement on the trailing car

The difference in magnitude of the drag changes can be explained by the reduction in the surface area on which the vortices impinge. This reduction in surface area causes a reduction in the overall pressure increase in front of the car compared to the Ahmed body. The wheels contribute to over 20% of the total drag generated. The impact of longitudinal spacing on the vortices generated off the wheels is negligible. This adds to the reduced drag change recorded in the DrivAer platoon case.
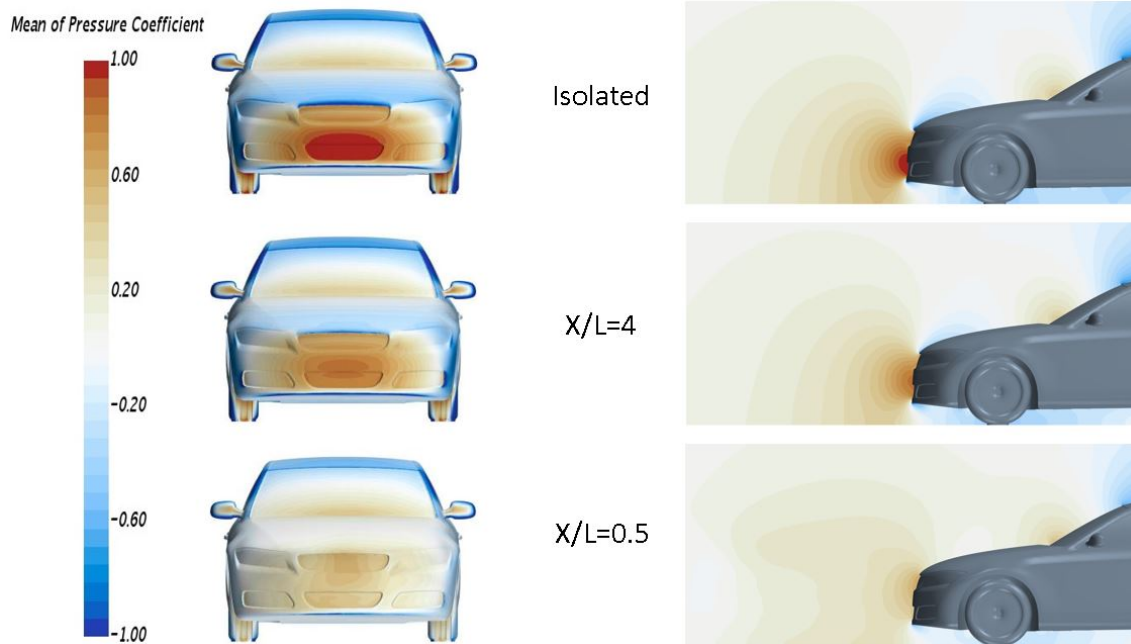
Figure 6.12: Surface pressure distribution on the frontal surface of the trailing car: Isolated(top), x/L=4(middle) and x/L=0.5(bottom)

Figure 6.12 shows the movement of the stagnation point along the nose of the trailing car compared with the stagnation point in the isolated model. The high pressure region marks the stagnation point. The stagnation point is not concentrated in a smaller area anymore as the trail car closes in on the front car. The overall pressure distribution in front of the car and over the hood increases.
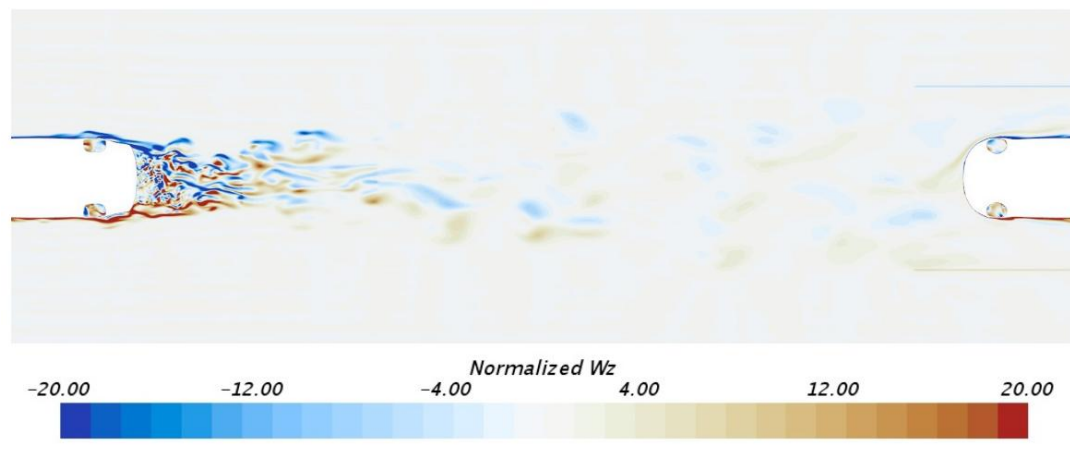
Figure 6.13: $\omega_Z{}^*$ along Z=0L plane showing vortices in the inter-vehicle spacing at x/H=4L
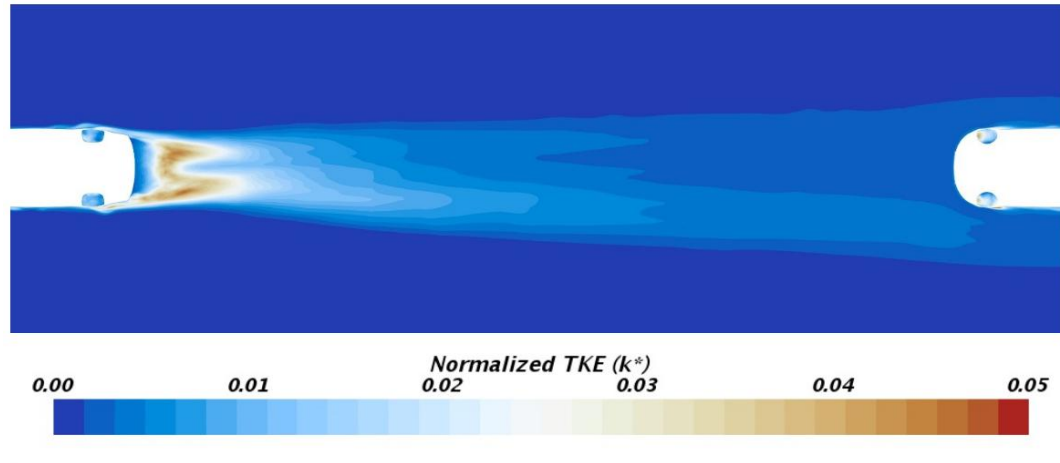
Figure 6.14: Normalized mean TKE along Z=0L plane showing lead model wake at x/H=4L

6.3   Concluding Remarks

The simulations to study the the predictability of interferences between ground vehicles was conducted with a detailed geometry of the factback variant of DrivAer reference geometry. Simulations revealed that the current models available can predict results of an isolated model almost identical to experimental results when tuned promptly. A few flow interaction phenomena are validated such as the vortex impingement. At closer spacings, the leading car benefits significantly from the interactions while the trailing car's drag increases. The drag penalties are not as steep as predicted by Ahmed body studies[4, 31]. This is due to reasons such as the wake from the wheels remaining unaffected with the change in spacing, reduced surface area for impingement and the wake length differences between the Ahmed model and the DrivAer model. The trailing car wake remain unaffected through the different spacings as recorded by previous platooning studies. With the current computational availability, it is close to impossible to use LES simulations or DNS simulations to study vehicle interferences. Hence, IDDES is the best possible way to study this particular case. Further investigations on the far wake resolution of such detailed geometries is absolutely necessary as the need for data on such scenarios is much needed.

CHAPTER 7: CONCLUSIONS

This final chapter is a summary of the research performed herein and restates important conclusions reached in the study. This research work focused on investigating the prediction capabilities of popular turbulence models in simulating bluff bodies and realistic car geometries in isolation and in a convoy arrangement. The author developed a simulation methodology based on prior literature knowledge and by simulating multiple case setups on a surface-mounted cube until an optimum method was reached. This initial testing phase was conducted only on a surface-mounted cube considering the availability of computational resources and the ease to validate the results against a plethora of experimental and numerical data available from previous literature. After the process was scrutinized, the same methodology was applied to a realistic ground vehicle geometry, the DrivAer model, and the platooning case was studied. Major conclusions from each test phase have been reported in their respective sections. Here, the conclusions on the overall prediction capabilities of the turbulence models in modeling vehicle interferences are being summarized.

- The initial step in this research work was to develop the meshing strategy that is capable of capturing the salient flow features around a bluff body and then identify a turbulence model that has the best prediction capability.

- After testing multiple test cases, a meshing strategy was obtained where the numerical calculations are no longer influenced by mesh refinement.

- The SST Menter k-ω model was observed to produce the best correlated predictions of flow past an isolated bluff body. It was then used in all subsequent

quasi-steady simulations investigating multiple bluff body aerodynamic interactions.

- In spite of have the best predictive capability among the chosen models, the default SST model over-predicts the shear layers separating off the leading face of the cube and hence over-predicts the recirculation region at the base of the bluff body.

- The influence of turbulence model closure coefficients on the predictions capabilities were tested and a combination of modified coefficients was reached. The combination improves the overall predictions of the SST model.

- After analyzing flow fields around the surface-mounted cube predicted by the URANS and IDDES-SST models, it was clear that URANS models faces issues in resolving the far wake. The flow never relaminarizes and, hence, the wake extends to an infinite distance behind the cube.

- The flow predictions from the IDDES-SST model were compared and contrasted against experimental and DNS results[16, 17, 22]. The flow features and velocity profiles were captured extremely well.

- Results from the tandem cubes simulations using IDDES-SST were compared against Martinuzzi's work[25, 24]. The trends of force coefficients predicted in the current study matched the results of Martinuzzi. The flow in the wake as well as the inter obstacle gap are captured with a reasonable accuracy.

- A CFD model to study the fastback variant of the DrivAer model was then developed using the information gathered from the simulations on surface-mounted cube.

- The only model used for this study was the IDDES-SST model. The modi-

fications of closure coefficients improve the predictions similar to the surface-mounted cube case.

- The drag coefficient predictions were within 3% of experimental values after applying the corrections for restraint as suggested by Collin et al.[38].

- The predicted flow features matched the results of Heft et al.[1]. The A-pillar vortex, which is usually over predicted in default turbulence models, was corrected with the modifications to the closure coefficients.

- The pressure distribution over the surface of the DrivAer model matched well with the experimental results, although the Cp on the roof centerline near the rear windshield in underestimated. This underestimation might be due to the absence of stinger or a difference in the manufactured DrivAer's windshield-roof transition. A similar under prediction was reported by other studies on the DrivAer model as well. The pressure recovery over the hood and the adverse pressure gradients over the windshield to the trunk lid are captured well.

- In platoon, the drag changes experienced by both the DrivAer models are similar in trend when compared to Pagliarella's results[4]. The drag of the lead car decreases and the drag of the trail car increases with decrease in longitudinal spacing. The change in drag is almost linear throughout the spacings.

- This is due to vortex interactions in the inter-vehicle spacings as described by Pagliarella[4]. The current study supports vortex impingement on the front surface of the trailing car. The stagnation point on the nose surface moves upward and the total pressure distribution in the inter-vehicle spacing increases with reduction in spacing.

- The trailing car does not return to an isolated state at a spacing of 4 car lengths. The wake of the DrivAer model extended longer than the Ahmed body wakes.

- The magnitude of the the drag changes are smaller than the Ahmed body predictions. This is due to the following reasons:

  - The wake is longer, more than 4 car lengths behind the model's base, and is made more turbulent by the intricate details of the geometry and hence affects the flow reaching the trail model.

  - The wheels contribute to over 20% of the total drag. The wake of the wheels seem unaffected by the change in inter-vehicle spacing. Hence, the total drag change is not as pronounced.

  - Unlike the Ahmed body, the DrivAer model does not have a flat frontal surface. The reduced surface area available for impingement causes diminished magnitude of drag change.

- Hence, one-to-one comparison cannot be made between Ahmed bodies and actual road vehicles. There is a clear difference in the drag predictions due to the influence of the intricate geometric details in an actual vehicle geometry.

These observations show that with the capabilities of present day turbulence models, predictions can be considerably improved to match experimental data and hence can be used for repeatability in the design process. This would save a huge amount of time and monetary resources. The study also underlines the deficiencies of URANS modeling in resolving far wakes even for simple geometries. IDDES-SST model shows promise in resolving complex wake flows. URANS simulations can be used in simulating an isolated vehicle for cases in which far wake resolutions are of lesser concern. Ahmed bodies can only be used to understand broad trends in such platooning scenarios as there is a considerable difference in the magnitude of predictions.

With this study highlighting the issues with current day turbulence models and their dependence on grid resolution, a grid refinement study can be done to determine the extent to which grid refinements affect the far wake calculations. Although, this

would require huge computational resources and lots of time. The effect of closure coefficients can be tested on other DrivAer model variants and an optimum set can be found. Different platoon configurations can be studied with different variants in the platoon or increasing the number in a platoon. Transient cases can be simulated to understand the influence of relative velocity and can be compared to the studies done using Ahmed bodies.

REFERENCES

[1] A. I. Heft, T. Indinger, and N. A. Adams, "Introduction of a new realistic generic car model for aerodynamic investigations," tech. rep., SAE Technical Paper, 2012.

[2] S. E. Shladover, "Longitudinal control of automated guideway transit vehicles within platoons," *Journal of Dynamic Systems, Measurement, and Control*, vol. 100, no. 4, pp. 302–310, 1978.

[3] W.-H. Hucho, "Aerodynamics of road vehicles: From fluid mechanics to vehicle engineering, w," *SAE International, Warrendale, PA*, vol. 177, 1998.

[4] R. Pagliarella, *On the aerodynamic performance of automotive vehicle platoons featuring pre and post-critical leading forms*. PhD thesis, 2009.

[5] C. Noger, C. Regardin, and E. Szechenyi, "Investigation of the transient aerodynamic phenomena associated with passing manoeuvres," *Journal of Fluids and Structures*, vol. 21, no. 3, pp. 231–241, 2005.

[6] S. Watkins and G. Vino, "The effect of vehicle spacing on the aerodynamics of a representative car shape," *Journal of wind engineering and industrial aerodynamics*, vol. 96, no. 6-7, pp. 1232–1239, 2008.

[7] A. Watts, "Computational characterization of drag reduction for platooning heavy vehicles," *Masters Thesis*, 2015.

[8] P. Gillieron and C. Noger, "Contribution to the analysis of transient aerodynamic effects acting on vehicles," tech. rep., SAE Technical Paper, 2004.

[9] R. Corin, L. He, and R. Dominy, "A cfd investigation into the transient aerodynamic forces on overtaking road vehicle models," *Journal of Wind Engineering and Industrial Aerodynamics*, vol. 96, no. 8-9, pp. 1390–1411, 2008.

[10] A. D. Chellaram, "Simulation of an overtaking maneuver using simplified vehicle bodies," 2016.

[11] A. I. Heft, T. Indinger, and N. A. Adams, "Experimental and numerical investigation of the drivaer model," in *ASME 2012 Fluids Engineering Division Summer Meeting collocated with the ASME 2012 Heat Transfer Summer Conference and the ASME 2012 10th International Conference on Nanochannels, Microchannels, and Minichannels*, pp. 41–51, American Society of Mechanical Engineers, 2012.

[12] W.-H. Hucho, "The aerodynamic drag of cars current understanding, unresolved problems, and future prospects," in *Aerodynamic drag mechanisms of bluff bodies and road vehicles*, pp. 7–44, Springer, 1978.

[13] G. Romberg, F. Chianese, and R. Lajoie, "Aerodynamics of race cars in drafting and passing situations," tech. rep., SAE Technical Paper, 1971.

[14] A. Heft, T. Indinger, and N. Adams, "Investigation of unsteady flow structures in the wake of a realistic generic car model," in *29th AIAA Applied Aerodynamics Conference*, p. 3669, 2011.

[15] S. R. Ahmed, G. Ramm, and G. Faltin, "Some salient features of the time-averaged ground vehicle wake," *SAE Transactions*, pp. 473–503, 1984.

[16] H. J. Hussein and R. Martinuzzi, "Energy balance for turbulent flow around a surface mounted cube placed in a channel," *Physics of Fluids*, vol. 8, no. 3, pp. 764–780, 1996.

[17] A. Curley, M. Uddin, and B. Peters, "Direct numerical simulation of turbulent flow around a surface mounted cube," in *22nd AIAA Computational Fluid Dynamics Conference*, p. 3431, 2015.

[18] R. Martinuzzi and C. Tropea, "The flow around surface-mounted, prismatic obstacles placed in a fully developed channel flow (data bank contribution)," *Journal of Fluids Engineering*, vol. 115, no. 1, pp. 85–92, 1993.

[19] J. Hunt, C. Abell, J. Peterka, and H. Woo, "Kinematical studies of the flows around free or surface-mounted obstacles; applying topology to flow visualization," *Journal of Fluid Mechanics*, vol. 86, no. 1, pp. 179–200, 1978.

[20] I. Castro and A. Robins, "The flow around a surface-mounted cube in uniform and turbulent streams," *Journal of fluid Mechanics*, vol. 79, no. 2, pp. 307–335, 1977.

[21] W. Rodi, "Comparison of les and rans calculations of the flow around bluff bodies," *Journal of wind engineering and industrial aerodynamics*, vol. 69, pp. 55–75, 1997.

[22] A. Yakhot, H. Liu, and N. Nikitin, "Turbulent flow around a wall-mounted cube: A direct numerical simulation," *International journal of heat and fluid flow*, vol. 27, no. 6, pp. 994–1009, 2006.

[23] P. W. Bearman and J. C. OWen, "Reduction of bluff-body drag and suppression of vortex shedding by the introduction of wavy separation lines," *Journal of Fluids and Structures*, vol. 12, no. 1, pp. 123–130, 1998.

[24] R. J. Martinuzzi and B. Havel, "Vortex shedding from two surface-mounted cubes in tandem," *International journal of heat and fluid flow*, vol. 25, no. 3, pp. 364–372, 2004.

[25] R. J. Martinuzzi and B. Havel, "Turbulent flow around two interfering surface-mounted cubic obstacles in tandem arrangement," *Journal of fluids engineering*, vol. 122, no. 1, pp. 24–31, 2000.

[26] N. Lindener, H. Miehling, A. Cogotti, F. Cogotti, and M. Maffei, "Aeroacoustic measurements in turbulent flow on the road and in the wind tunnel," tech. rep., SAE Technical Paper, 2007.

[27] Y. Nakamura, "Bluff-body aerodynamics and turbulence," *Journal of Wind Engineering and Industrial Aerodynamics*, vol. 49, no. 1-3, pp. 65–78, 1993.

[28] A. A. Azim, "An experimental study of the aerodynamic interference between road vehicles," tech. rep., SAE Technical Paper, 1994.

[29] K. Götz, T. Casey, J. Bacon, *et al.*, "Bewegungssehen und flugsteuerung bei der fliege drosophila," in *Symposium Physiology and Biophysics of Insect Flight 1982*, pp. 21–34, Akademie der Wissenschaften und der Literatur, 1983.

[30] A. F. A. Azim and A. F. A. Gawad, "A flow visualization study of the aerodynamic interference between passenger cars," tech. rep., SAE Technical Paper, 2000.

[31] G. Rajamani, "Cfd analysis of air flow interactions in vehicle platoons," 2006.

[32] D. C. Wilcox *et al.*, *Turbulence modeling for CFD*, vol. 2. DCW industries La Canada, CA, 1998.

[33] B. Peters, *On Accelerating Road Vehicle Aerodynamics*. PhD thesis, 2018.

[34] B. E. Launder and D. B. Spalding, "The numerical computation of turbulent flows," in *Numerical Prediction of Flow, Heat Transfer, Turbulence and Combustion*, pp. 96–116, Elsevier, 1983.

[35] D. C. Wilcox, "Formulation of the kw turbulence model revisited," *AIAA journal*, vol. 46, no. 11, pp. 2823–2838, 2008.

[36] F. R. Menter, M. Kuntz, and R. Langtry, "Ten years of industrial experience with the sst turbulence model," *Turbulence, heat and mass transfer*, vol. 4, no. 1, pp. 625–632, 2003.

[37] J. Paik, F. Sotiropoulos, and F. Porté-Agel, "Detached eddy simulation of flow around two wall-mounted cubes in tandem," *International Journal of Heat and Fluid Flow*, vol. 30, no. 2, pp. 286–305, 2009.

[38] C. Collin, S. Mack, T. Indinger, and J. Mueller, "A numerical and experimental evaluation of open jet wind tunnel interferences using the drivaer reference model," *SAE International Journal of Passenger Cars-Mechanical Systems*, vol. 9, no. 2016-01-1597, pp. 657–679, 2016.

[39] C. Strangfeld, D. Wieser, H.-J. Schmidt, R. Woszidlo, C. Nayeri, and C. Paschereit, "Experimental study of baseline flow characteristics for the realistic car model drivaer," tech. rep., SAE Technical Paper, 2013.